Economic optimisation of distributed energy storage

inw.

Technische Universiteit
Eindhoven
University of Technology

Electrical Energy Systems
Department of Electrical Engineering
Den Dolech 2, 5612 AZ Eindhoven
P.O. Box 90159, 5600 RM Eindhoven
The Netherlands
www.tue.nl

Author:
Garoufalis Panagiotis

Student ID:
843036

Supervisors:
Prof.ir. W.L.Kling
I.Lampropoulos

Reference
EES.13.A.0013

Date
September 2013

Economic Optimisation of Distributed Energy Storage

Panagiotis Garoufalis

Where innovation starts

Table of contents

The list in the table below includes the main notation of the thesis for quick reference. Other symbols are defined throughout the text.

Nomenclature

a, b, c, d	Indices for network connection points in the investigated system (See figure 1)
h	Index for the day-ahead market periods, $h = 1,...,24$
i	Discrete step for control periods, $i = 1,...,n$
t	Index for control periods, $t = 1,...,1440$
k	Current discrete time control period
l	Index for settlement periods, $l = 1,...,96$
m	Discrete step for settlement periods, $m = 1,...,48$
$P_b^{ihs}(h)$	Intra-hour (power deviation) schedule (W) at network point (b)
$E_a^{das}(h)$	Day-ahead (energy) schedule (Wh) at network point (a)
E_{nom}	Battery nominal capacity (Wh)
$P(k+i\|k)$	Predicted power trajectory (W) at time instant k
$P_a^{das}(h)$	Day-ahead (power) schedule (W) at network point (a)
$P_c^{das}(h)$	Day-ahead (power) schedule (W) at network point (c)
q	Current settlement period
$SoE(k)$	State of Energy (%) at time instant k
$\|S_a(k)\|$	Apparent power (VA) at network point (a) and at control period k
$\Delta E(l)$	Energy imbalance (Wh)
n_{ch}	Efficiency factor during the charging process (-)
n_{dis}	Efficiency factor during the discharging process (-)
$\Theta(h)$	Day-ahead cost function (€)
$\pi(h)$	Day-ahead market clearing price (€/Wh)
τ, $\tau_{horizon}$, τ_s, τ_h	Time intervals (s)

Chapter 1 Introduction

1.1. Energy and the environment

In the advent of the 21st century climate change appears to be one of its great challenges. Demand for energy and associated services, to meet social and economic development and improve human welfare and health, is continuously increasing. All societies require energy services to meet their basic human needs and to serve productive processes. Since approximately 1850, global use of fossil fuels (coal, oil and gas) has increased to dominate energy supply, leading to a rapid growth in carbon dioxide (CO2) emissions [1].

It is reported that fossil fuels provided 81.2% of the total primary energy in 2008, while the combustion of fossil fuels accounted for 56.6% of all anthropogenic greenhouse gas (GHG) emissions (CO_2 equivalent) [2]. GHG emissions associated with the provision of energy services are a major cause of climate change. Most of the observed increase in global average temperature since the mid-20th century is very likely due to the observed increase in anthropogenic greenhouse gas concentrations [3]. The rate of growing of the CO_2 concentrations are a major concern, while the warming trend has increased significantly over the last 50 years.

Furthermore, the exploitation of the reserves of fossil-based resources is currently occurring at a high rate. As far as crude oil is concerned, the maximum point of extraction i.e. the so-called peak oil has already been exceeded and the security of supply appears to be a serious concern[1]. At the same time the capacity of the earth's atmosphere to absorb greenhouse gases is limited, and any excess will stretch the impacts of climate change beyond manageable limits [4].

The climate change may have adverse impacts on water resources, ecosystems, food security, human health and coastal settlements with potentially irreversible abrupt changes in the climate system.

In order to maintain both a sustainable economy that is capable of providing essential goods and services to the citizens of both developed and developing countries, and a supportive global climate system, a major shift in how energy is produced and utilized is required [3],[5]. Towards that direction, renewable energy technologies have emerged as important options to mitigate supply problems and also simultaneously aid economic development.

Renewable energy (RE) (wind power, solar power, hydro energy, energy from the ocean, geothermal, biomass and biofuels) are alternatives to fossil fuels and help reduce greenhouse gas emissions, diversify energy supplies and reduce dependence on unreliable and volatile fossil fuel markets, especially oil and gas. The advantages associated with renewable energy technologies are numerous due to their replenishing nature, the emission of significantly lower amounts of CO_2 and their supportive character towards energy self-sufficiency of remote and developing regions. Moreover, such technologies can be applied for the development of flexible applications where power can be generated according to the needs of the on-site population, eliminating the need for huge power plants running on fossil fuel.

[1] http://www.worldenergyoutlook.org/media/weowebsite/2009/weo2009_es_english.pdf

1.2. Integration of renewable energy sources

Renewable energy refers to energy resources which are continually replenished such as sunlight, wind, rain, tides, waves and geothermal heat. Renewable energy sources reflect the time-varying nature of the energy flows in the natural environment, thus their power generation characteristics are very different in general from other generation based on stockpiles of fuel (with the exception of biomass-fuelled plants).

In 2008, RE contributed approximately 19% of global electricity generation. The contribution of RE to primary energy supply varies substantially by country and region. Future scenarios of low greenhouse gas systems consider RE both in standalone modes but also in combination with nuclear, and coal and natural gas with carbon capture and storage.

While the RE share in global energy use is still relatively small, deployment of associated technologies has been increasing rapidly in recent years. Out of the approximately 300 GW of new electricity generation capacity added globally over the two-year period from 2008 to 2009, 140 GW came from RE technologies. Collectively, developing countries hosted 53% of global RE power generation capacity in 2009 [6]. Under most conditions, increasing the share of RE in the energy mix will require policies to stimulate changes in the energy system. Government policy, the declining cost of many RE technologies, changes in the prices of fossil fuels and other factors have supported the continuing increase in the use of RE. These developments suggest the possibility that RE could play a much more prominent role in both developed and developing countries over the coming decades [6].

However, developing renewable resources appear to have some characteristics which raise a new set of technological challenges not previously faced within established power systems.

Some of the characteristics of distributed energy resources and renewable energy sources is their variability, unpredictability and intermittency. Variable energy sources produce fluctuating and (partly) unpredictable amounts of electricity over time. Intermittency inherently affects solar and wind energy, as the power generation from such sources depends on the amount of solar irradiation or the wind speed in a given location. Apart from that, the unpredictability associated with renewable generation, primarily caused by unanticipated weather conditions, such as clouds or sudden shifts in wind velocity is a major challenge for the integration of renewable energy resources in the power system.

Furthermore, the variability of renewable energy is easily accommodated when demand and renewable supply are matched, e.g., both rising and falling together. However when demand and renewable supply move in opposite directions, the cost of accommodation can rise significantly.

As renewable energy penetration grows, the increasing mismatch between variation of renewable energy resources and electricity demand makes it necessary to capture electricity generated by wind, solar and other renewable energy generation for later use. Energy storage is a possible technical solution to help smooth fluctuations in generation inherent in RE such as wind or solar energy.

1.3. Energy storage

Energy storage technologies can be used to store electricity, which is produced at times of low demand and low generation cost, and from intermittent energy sources such as wind and solar. Stored energy can be released at times of high demand and high generation cost or when there is limited base generation capacity available.

Reliable and affordable energy storage is a prerequisite for using renewable energy in remote locations, for the integration into the power system and the development of a decentralised energy supply system in the future. Furthermore, these concepts straightforwardly extend to the use of traditional fossil fuel-based generation. Energy storage therefore has a pivot role to play in the effort to combine a future sustainable energy supply with the standard of technical services and products that were accustomed to. In this way, energy storage is the most promising technology currently available to reduce fuel consumption, and supports the new paradigm of electrical microgrids operation by permitting distributed generation to seamlessly operate as a dispatchable unit and autonomously isolated from the main power system [7].

Energy storage solutions can provide a considerable option for the integration of renewable energy sources and the establishment of efficient generation and delivery of electrical power. For almost half century there have been dedicated research and development efforts to introduce batteries to the electric utility industry, in a load levelling mode, for the large scale integration of renewable energy sources. Early studies indicated the unique role that integrated battery and photovoltaic (PV) systems can play in demand side management (DSM) activities, and that those developments will most likely impact the deregulation of electrical power systems [8], [9], [10].

DSM refers to the modification of the consumer's energy demand through various methods (i.e. financial incentives). It addresses a range of functions including program planning, evaluation, implementation and monitoring [11]. Demand response (DR) is a term used in economic theory to identify the short-term relationship between price and quantity. Currently the term is used in a broad sense, as a part of DSM, and is attributed to a variety of control signals such as prices, resources availability and network security [12].

Energy storage can be implemented in large-scale (e.g. pump-hydro etc.) but also in a distributed fashion. A distributed battery system along with distributed generators (DGs) and flexible loads is a resource that falls under the general term of DSM.

A battery energy storage system (BESS) is defined as [7]: "An energy storage system using shunt connected, voltage sourced converters capable of rapidly adjusting the amount of energy that is supplied to or drawn from the ac system. The reactive power generating or absorbing capability of the voltage sourced converter can be utilised to generate a capacitive or inductive component of output current independent of the flow of real power and within the limits of the converter rating".

In the technical literature, numerous potential applications have been defined for BESS in planning and operation of electrical power systems. The main drivers for the developments of energy storage are market opportunities through energy arbitrage, the provision of ancillary services to the system, efficiency improvements of generation, transmission and distribution assets, integration of intermittent renewable energy resources by firming up the service, remote area power supply and multiple complementary applications [7]. The latter point actually signifies that a single

application of energy storage is unlikely to provide economic justification, however the possibility of changing storage control strategies depending on the market requirements could allow maximisation of revenues [7].

In the Netherlands, research related to the impact of BESS on electricity distribution systems with stochastic generation was initiated with the Bronsbergen microgrid project [13]. The Bronsbergen microgrid is operated by the distribution system operator (DSO) Alliander and consists of a distribution system connecting 210 residences, of which 108 are equipped with PV generators (total installed capacity of 315 kWp). The research activities related to the Bronsbergen microgrid addressed the topics of islanded operation (maintaining islanded mode for 24 hours, automatic isolation from and reconnection to MV network), black start and power quality phenomena.

Enexis DSO developed and commissioned a BESS to enable field-testing and research of advanced energy storage technologies in LV distribution grids. The BESS was installed in the LV distribution grid for the purpose of enabling applications such as, but not limited to: the increase of local PV consumption, improvement of reliability and flexibility, reduction of losses, and maximizing the utilization of local infrastructure [14]. A schematic of the investigated case study is depicted in Fig.1.1, and consists of an actual distribution system with integrated energy storage in Etten-Leur, the Netherlands. The implemented BESS is connected to the LV-side of a local 400 kVA MV/LV transformer (0.4 / 10 kV) station operated by Enexis DSO, with an average peak-load measured at 385 kW at the moment of installation. Approximately 240 households are connected to this MV/LV station from which 40 houses have locally installed PV modules (in total 186 kWp).

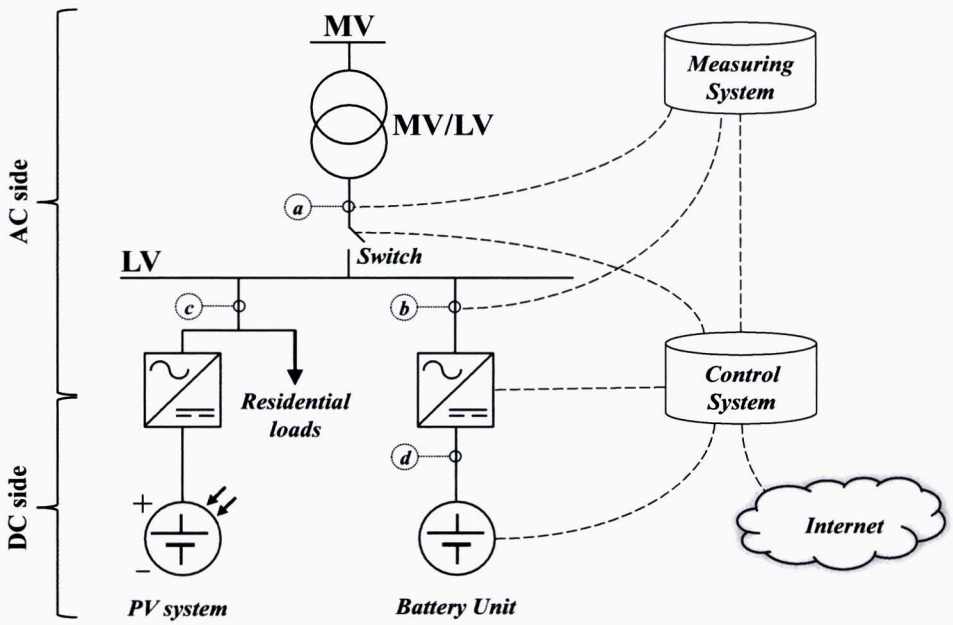

Figure 1.1 The system architecture illustrating the single line diagram of the physical power system network and a schematic of the control architecture. The solid black lines depict the physical power network, while the dashed lines represent the information and communication network.

1.4. *Problem definition*

The BESS in Etten-Leur serves as a case study in this investigation. It was built in order to gain operational experience and to facilitate research on the impact of storage in the electricity grid at the distribution level [15].

Throughout this thesis, the economic optimisation of the BESS through the application of optimisation techniques is studied. The work looks at possible markets for small-scale, grid-connected electricity storage in a liberalised market setting. Specifically, it addresses the interactions of the system with the day-ahead electricity auction and the real time balancing market in the Netherlands. A more thorough description of these markets is provided in Section 2.1.

For analysing the response of the aggregate DR system, the developed simulation scenario focuses on the Netherlands and covers a period of 24 hours. During the *day-ahead* operational planning (*a priori*), the timescale corresponds to discrete time periods τ_h of 1 hour, in line with the defined *day-ahead* market settlement periods in the Netherlands. At the intra-hour planning, the timescale corresponds to discrete time periods of 15 minutes, in line with the defined settlement periods for imbalance energy verification and settlement in the Netherlands. During real-time operation, the time interval for simulations and for sampling analogue measurements is set to 1 min., inspired by the current implementation of the BESS in *Etten-Leur*.

Figure 1.2 Photo of the Smart Storage Unit (SSU), as it is installed in the field at Etten-Leur.

The underlying business model in the developed scenario sets distinct roles among all system actors. The aggregator is representing all the connected entities to the LV bus, i.e., the residential customers, the PV installations and the BESS. The residential users and the photovoltaic generators are aggregated in a community way and are not participating separately in the markets. Moreover, throughout the whole thesis, the case study is considered to be small enough so that it does not influence the market clearing price (MCP). The interactions between the system actors during the *day-ahead* planning phase, the real-time operations, and the verification process are further discussed in the following paragraphs.

The specifications of the Etten-Leur case study are presented in Table 1.1.

Table 1.1 Specifications of the Etten-Leur Case Study [14], [16],[17].

Main characteristics	Value	Unit
THE LOW VOLTAGE DISTRIBUTION GRID		
Grid Connection Nominal Voltage [a]	400	V
Transformer Capacity	400	kVA
Average Peak Load Measured [b]	385	kW
Number of Households	240	-
Installed PV capacity	186	kW_p
THE BATTERY ENERGY STORAGE SYSTEM		
Nominal Voltage	730	V
Minimum (Discharge) Voltage	609	V
Maximum (Charge) Voltage	812	V
Nominal Capacity	230	kWh
Nominal Capacity [c]	328	Ah
Minimum Capacity [c]	312	Ah
Maximum Discharge Power [d]	400	kW
Nominal Discharge Power	400	kW
Maximum Charge Power [e]	400	kW
Nominal Charge Power	100	kW
Operating temperature range	−20 to +60	°C

[a] Line to line voltage
[b] At the moment of installation around October 2012
[c] Rating C/3 at 25°C
[d] For thirty minutes
[e] Only for a few seconds

The approach is based on hierarchical decomposition of the control problem in the time domain, by composing a three-level optimisation problem, i.e., day-ahead, intra-hour and real-time, where the initial and final states of each sub-problem are chosen as coordination parameters.

1.5. Scope of work

The scope of this work is to define a viable control scheme for the real-time management of the residential customers, the PV system and the BESS connected to the LV grid operated by Enexis DSO, based on the application of economic optimisation techniques.

The control scheme is responsible for the management of the aggregator in order to benefit by participating in the APX day-ahead and the Tennet imbalance market.

The work examines the possibility of maximising the revenues or minimising the losses by changing the control strategy of the BESS subject to the market requirements.

1.6. Layout of the thesis

The first chapter includes an introduction presenting the existing environmental situation, the RE development and the integration challenges, as well as the problem definition, the scope of work and the layout of the thesis.

In Chapter 2, a description of the system architecture is provided, including an overview of the electricity markets in the Netherlands and a description of the system actors.

Chapter 3 describes the day-ahead problem. The day-ahead operational planning is presented first, followed by the results of the developed optimisation approach. An economic analysis for several years is provided along with discussion for the relation of the annual revenues of the system under the specified application and the historical volatility of the day-ahead market in the Netherlands.

Chapter 4 addresses the interactions with the balancing energy market in the Netherlands and the intra-hour scheduling approach. The intra-hour scheduling approach is explained and the results of the optimisation problem are presented. Several cases studies are examined including prediction errors with respect to the forecasts of the power profile and market prices.

Chapter 5 describes the real-time problem (i.e. real-time operations under uncertainty and fast changing conditions) and includes the real-time planning and the results of the optimisation algorithm for the same cases that were studied in Chapter 4.

In Chapter 6, the conclusions of this study are drawn based on analysis of the overall results (i.e. for all the investigated simulation scenarios of the day-ahead, intra-hour and real-time problems). The report ends with recommendations for future research.

Chapter 2 System Architecture

In this chapter, the architecture of the system under investigation is described. First, an overview of electricity markets is provided, defining those procedures and parameters that are relevant for the problem formulation (Section 2.1). In the second part of this chapter (Section 2.2) the physical layer of the investigated system is described. The physical system can be distinguished between the physical power system (i.e. the electricity distribution system including the BESS the residential customers and the PV installations) and the physical ICT infrastructure (i.e. the measuring equipment and communication links). The third part (Section 2.3) addresses the basic logic behind the control approach, whereas the modelling of the system is presented at the last section of this chapter (Section 2.4)

2.1. Electricity Markets in the Netherlands

2.1.1. Overview

The Dutch electricity market has been fully open to competition since July 2004 [18] and from that date, small consumers were free to choose their own electricity supplier. In the Netherlands, market parties can trade electrical energy, and these transactions are executed by establishing bilateral contractual purchase and sale relationships within power exchanges. Currently, there are several markets for trading energy in the Dutch system; forward (or bilateral) market, day-ahead and intraday spot markets (also called wholesale markets), and a single buyer energy imbalance market (which is essentially an ancillary services market). Apart from these markets, there is the imbalance settlement mechanism which is called the day after the operational day.

The different markets that exist for trading electricity, can be categorised as:

- Forward Markets (based on bilateral trade and anonymous trade through a power exchange)
- Spot Markets (Day ahead and intra-day auction markets, also called wholesale markets)
- Ancillary Services Markets (Congestion avoidance, voltage regulation, and energy reserves for power balancing etc.)

In this study, the focus is on the APX day-ahead auction and the balancing energy market operated by Tennet, the Dutch Transmission System Operator (TSO), which are further described in the following sections [19].

2.1.2. The APX day-ahead market

Spot Markets refer mainly to the central exchange of electrical energy for the preceding day of the day that the actual production and physical delivery takes place.

At the day–ahead auction, trading takes place on one day for the delivery of electricity on the following day. Market members submit their offers and orders electronically, after which supply and demand schedules are compared and the market price is calculated for each hour of the following day.

The development of demand and supply curves on the APX spot market is completely determined by the market parties themselves. Players are production and distribution companies, large consumers, industrial end-users, brokers and traders. All of these can be active as buyers or suppliers. The bids from buyers and sellers must be made known to APX one day in advance. After the closure of the day-ahead bidding, APX provides matching and sends the result to the bidders [20].

The hourly instruments that the members can trade, are traded for each hour of the delivery day. Individual hourly instruments are traded in Euro/MWh with a precision of two decimals.

APX is the central counterparty to all trades; all contracts are traded anonymously, then cleared and settled on behalf of the members. Contracts on the exchange are fully collateralised, as all members are required to lodge collateral. All trades are notified to the Dutch Power grid operator TenneT BV by double-sided nominations, to be sent by APX and the trading member.

Fig. 2.1 depicts the timing of actions of the several markets, and it can be seen that the day-ahead bidding takes place on the previous day (D-1 in Fig.2.1.) and closes at the Gate Closure Time (GCT), at 12:00 pm.

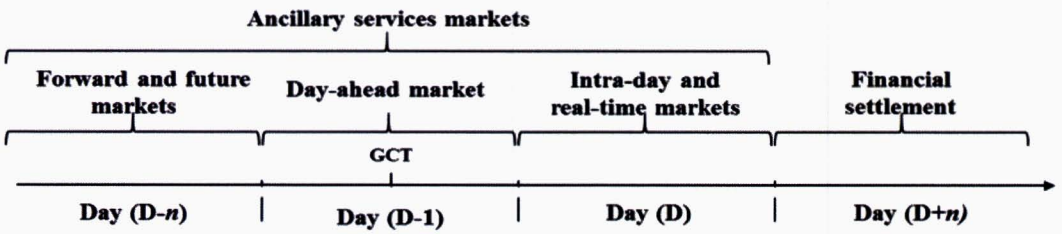

Figure 2.1 Timing of electricity markets in the Netherlands.

2.1.3. Imbalance Settlement System

In the Netherlands, TenneT, the national TSO, is the authorised entity to procure balancing services for maintaining the system balance. TenneT transfers part of this responsibility to market participants by implementing a system of programme responsibility. Market participants are acknowledged as Programme Responsible Parties (PRP) with the responsibility to keep their portfolio balanced for each settlement period. In the Netherlands, the settlement period is termed Programme Time Unit (PTU) and is defined in a 15 minutes basis. A PRP uses information from the imbalance settlement system to either act and internally solve its own imbalance, or to accept the adjustment imbalance by the TSO, or to contribute to system balancing without being actively selected via the bidding ladder (i.e. having an internal imbalance in the opposite direction of the system imbalance) [21]. This last form of participation to restore the system balance is also known as passive contribution and is rewarded in the Dutch balancing framework [22]. However, for the provision of operating reserve capacity by active contribution, TenneT acknowledges market entities that place bids in the market for operating reserves as Regulating and Reserve Power Suppliers (RRPS), and/or Emergency Power Suppliers (EPS) [23].

2.1.3.1. Active contribution

Following the clearing of the day-ahead market, each PRP submits its positions to the TSO in terms of energy schedules (e-programmes), one for each PTU of the day-ahead. These e-programmes include energy volumes traded and settled on the wholesale (forward, future and spot) markets. The TSO receives the e-programmes of each PRP and performs consistency checks. Furthermore, before approval, the TSO performs a network security analysis. Then, during operation, each PRP is subjected to adjustment imbalance (difference between actually allocated values and submitted positions in e-programmes). The TSO monitors the system imbalance on real-time and if needed calls bids for operating reserves to restore the system balance. The TSO might also contract on beforehand balancing capacity to ensure system security. Specifically, TenneT contracts a part of the operating reserve capacity with suppliers, from which the suppliers will have the obligation to offer this minimum capacity on the market for operating reserves. Finally, the financial imbalance settlement between the TSO and market parties occurs ex-post (i.e. after the operational day) [21].

2.1.3.2. Passive contribution

In the Dutch imbalance management system control area imbalance positions and imbalance price are made public in near real-time. Therefore all market participants have the opportunity to voluntarily contribute to the TSO efforts in maintaining the system balance. This approach is called 'passive contribution' ('passief meeregelen' in Dutch) and is believed to result in a substantial reduction in the required control energy [24]. TenneT, the Dutch TSO, publishes the Dutch system balance position and balance energy price near real-time. This information is used by market participants to actively reduce the system imbalance, utilizing non-contracted reserve power. The Dutch balancing mechanism seems likely to reveal higher-level macro-economic efficiencies and the passive contribution of decentralized market parties seems to create more competition without jeopardizing the system's stability [24].

TenneT publishes the table entitled 'Bid price ladder balancing' for each date and for each settlement period, which shows price information for bids of regulating and reserve power capacity offered to TenneT for real-time balancing[24].

The bid price ladder balancing can be used to a limited extent to estimate real-time settlement prices in combination with the 'Balance Delta' table. TenneT publishes the 'Balance delta' table which shows the quantities of regulating and reserve capacities (for each minute of the most recent half hour) that were requested for its operations [25].

An example of the bidding ladder for the imbalance settlement system is illustrated in Fig.2.1. The TSO monitors on real-time the system imbalance and selects bids for the imbalance settlement either for positive (ΔP_+) or negative (ΔP_-) reserves. In Fig.2.1, π_+ is the settled price for up-regulating balancing capacity ΔP_+, π_- is the price for down-regulating capacity ΔP_-, and π_{mid} is the price which corresponds to the mid price, i.e., the midpoint between the lowest bid price at the upward and the highest bid price at the downward regulating side. In the case of real-time imbalance, the TSO will call as many bids as necessary to restore the system balance, and finally all the service providers are paid the same price which is equal to the most expensive bid called.

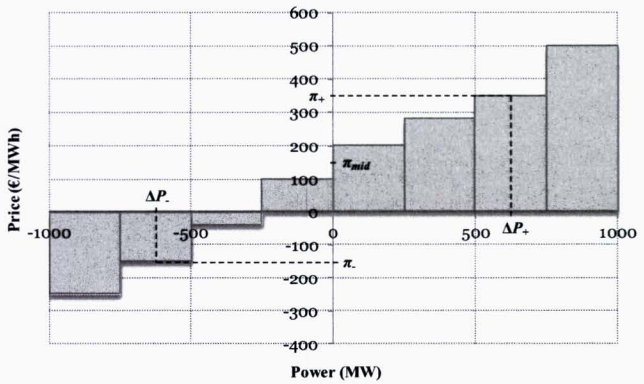

Figure 2.2 Schematic illustration of the bid price ladder for the imbalance settlement system in the Netherlands.

In Table 2.2, the price interdependencies for Program Responsible Parties (PRP) in the Dutch imbalance settlement system are presented. A PRP with a *surplus* (or *shortage*) faces an imbalance price π_{surpl} (or π_{short}) which is dependent on the system state. Let us denote the predicted system state for the *l*th settlement period as $s^{prd}(l) = \{0,1,-1,2\}$, where each value corresponds respectively to a balanced state '0', i.e., neither upward nor downward regulation, exclusively upward regulation '+1', exclusively downward regulation '−1', and both upward and downward regulation '2' [22]. The incentive component π_{ic} is the component of the imbalance price that is intended to encourage market parties to actually submit bids of regulating and reserve capacity used by TenneT to maintain and restore the balance, and as an incentive to minimise the imbalance to be settled. An analysis of the data for the year 2012, shows that the incentive component was non-zero for about 2.73 % of the total time [26].

Table 2.1 Price dependencies for Program Responsible Parties in the Dutch imbalance settlement system [23].

System State	Time (%) [d]	Regulation Actions	PRP Surplus (π_{surpl} for $\Delta E>0$)	PRP Shortage (π_{short} for $\Delta E<0$)
0	06.99	None	$\pi_{mid}-\pi_{ic}$	$\pi_{mid}+\pi_{ic}$
+1 (short)	36.27	Upwards [a]	$\pi_{+}-\pi_{ic}$	$\pi_{+}+\pi_{ic}$
−1 (long)	45.04	Downwards [b]	$\pi_{-}-\pi_{ic}$	$\pi_{-}+\pi_{ic}$
2	11.50	Bidirectional	$\pi_{-}-\pi_{ic}$	$\pi_{+}+\pi_{ic}$
+1, *em*[c] (short)	00.17	Upwards [a]	$\max(\pi_{+}, \pi_{em})-\pi_{ic}$	$\max(\pi_{+}, \pi_{em})+\pi_{ic}$
2, *em*[c]	00.03	Bidirectional	$\pi_{-}-\pi_{ic}$	$\max(\pi_{+}, \pi_{em})+\pi_{ic}$

[a] If $\pi_{+} > 0$, then the TSO pays the PRP, else the PRP pays the TSO.
[b] If $\pi_{-} > 0$, then the PRP pays the TSO, else the TSO pays the PRP.
[c] The acronym '*em*' indicates that '*emergency power*' was called.
[d] For the reference year 2012 [26].

It has to be noted that prices π_{+} and π_{-} can be either positive or negative which indicates the flow of payments from a PRP to the TSO and *vice versa*. For example, for negative volumes of control energy, positive price values refer to a payment from the PRP to the TSO, while negative values refer to a payment from the TSO to the market party. In the case that the system is *long*, during the lth settlement period, then a PRP has an interest to maintain an internal energy imbalance $\Delta E(l)<0$ whenever $\pi_{-}+\pi_{ic} < 0$. An analysis of TenneT data for the year 2012 shows that while the system was *long*, the latter condition was fulfilled for about 13.5 % of the total time [26].

Contrary, in the case that the system is *short*, during the lth settlement period, then a PRP has an interest to maintain an internal energy imbalance $\Delta E(l)>0$ whenever $\pi_{+}-\pi_{ic} > 0$. An analysis of TenneT data for the year 2012 shows that while the system was *short*, the latter condition was fulfilled for 100 % of the total time. This information indicates that there are opportunities for the aggregator to receive additional revenues through passive contribution in real-time balancing [26].

The imbalance settlement in the Netherlands for market parties that contribute through passive contribution is based on the net energy volumes of provided control energy per settlement period. According to the previous analysis, when the system state is explicitly *short* or *long* then certain market parties might try to minimise or maximise the net amount of energy traded per settlement period. In such a case, the provision of more regulating capacity than requested is simply passive contribution which is delivered at the party's own risk. Furthermore, such actions might jeopardize any contractual payments and slow down a possible increase in marginal price, thus have a negative economic impact for certain suppliers of operating reserves. At the same time, this can be beneficial for market parties that are subjected to deviations from their e-programmes since it can result in reduced prices for the imbalance adjustment. Even though the system state will be known only ex-post, still certain market parties can try to estimate the balancing situation on real-time based on the delta-signals and historical data, and thus benefit from passive balancing (e.g. up-regulation), but such a situation might lead to an increase in marginal price for control power in the opposite direction (e.g. down-regulation).

2.2. System Design

An electrical power system consists of different control areas interconnected through high voltage (HV) synchronous or asynchronous connections. In Europe, each control area is operated by the transmission system operator (TSO), the legal entity that monitors the electricity network, ensures the connections with other control areas, and organises the markets for operating reserves and cross-border capacity. Regional DSO companies connect individual customers to the grid and provide the distribution of electricity. Medium voltage (MV) electrical networks (i.e., 10 – 110 kV) are connected to low voltage (LV) networks through MV/LV transformer substations, which subsequently feed a large number of end-users at the LV level.

The main actors distinguished in this work are: the *system operators* (i.e., the operators of the electricity markets, and the transmission and distribution systems), the *aggregators* (legal entities that hold contracts with system users, represent them to markets and operators, and coordinate them in real-time), and the *system users* (e.g. producers and consumers). For the selected case study in *Etten-Leur*, the aggregator is representing all the connected entities to the LV bus, i.e., the residential customers, the PV installations and the BESS. In the next sections, a decentralised control structure with a global coordinator (i.e., the aggregator) is presented. The aggregator is the operator of a virtual power plant (VPP) which consists of an aggregation of distributed resources. The residential loads and the PV installations are considered non-controllable resources, while the BESS is actually the only controllable process in the considered case study.

2.2.1. Technical Description and Specifications of the Battery Energy Storage System

The BESS consists of four main building blocks, i.e., the battery unit, the power conversion system, the measuring system and the control system, which are further described in the following paragraphs.

2.2.1.1. The Measuring System

In this work, since bidirectional energy flows are considered, by convention it is assumed that power values are positive for the energy flows from the secondary conductor of the MV/LV transformer to the BESS and the residential loads. As can be seen in the single-line diagram of Fig. 1, four network points (*a*)–(*d*) are defined: points (*a*)–(*c*) are at the AC side of the network, whereas only *rms* values are considered, and point (*d*) is at the DC side. For simplicity, the AC and DC indexes are omitted from the equations in the following descriptions.

The measuring instruments consist of transducer devices which are applicable for the measurement of voltage and current in energy distribution systems [27]. As can be seen in Fig. 1, transducer devices, for measuring the voltages and currents, are installed next to the secondary conductor of the MV/LV transformer at *measuring point* (*a*) and at the point of connection of the inverter and the battery system at *measuring point* (*b*). In this arrangement it is possible to determine all relevant power flows in the investigated LV grid. The power at time instant k at the *coupling point* (*c*) of the residential customers

and the PV system can be calculated, while neglecting network losses, by using (2.1):

$$P_c(k) = P_a(k) - P_b(k) \qquad (2.1)$$

The 3-phase AC apparent power $|S_a|$ at network point (a) can be calculated by using (2.2):

$$|S_a(k)| = \sqrt{(P_a(k))^2 + (Q_a(k))^2} \qquad (2.2)$$

The implemented BESS is connected to the LV-side of a local 400 kVA MV/LV transformer (0.4 / 10 kV) station operated by Enexis DSO, with an average peak-load measured at 385 kW at the moment of installation. Considering a P-Q decoupled control scheme, and under the assumption that the reactive power is zero, then the capacity constraint related to the installed transformer can be written as follows:

$$|S_a(k)| \leq 400\ kVA \Rightarrow -400\ kW \leq P_a(k) \leq 400\ kW \qquad (2.3)$$

2.2.1.2. The Battery Unit

The battery unit consists of a number of lithium-ion battery modules in series and parallel connections. Each module contains 14 cells which are assembled in two parallel strings, whereas each string is composed by 7 cells in series. This configuration results to a nominal voltage potential of 24 V and capacity of 2 kWh per module [17]. The BESS consists of four parallel battery strings, with each string comprising 29 lithium-ion battery modules in series. Each battery string has a 730 V nominal battery with a rated energy capacity of 57 kWh and is connected to a Battery Management Module (BMM). This provides electronic control of the 29 individual battery modules in charge and discharge and monitors their state of charge (*SoC*), state of health (SOH) and other operational data such as temperature. The four parallel battery strings are controlled by a Master Battery Management Module (MBMM). Its main function is to ensure that there is an equal *SoC* in all parallel strings and if unbalance is detected, or for maintenance purposes, it can bypass one or several strings. This is a critical feature for Li-ion battery architecture that prevents undesired discharges between strings, as well as enabling strings at a different *SoC* to be connected during installation or maintenance. The MBMM provides the control interface with the Power Conversion System. The total capacity of the BESS is about 230 kWh, whereas the power charging and discharging rate is 200 kW (only seconds) and 400 kW (30 min.) respectively.

2.2.1.3. The Power Conversion System

The power conversion system, depicted between points (*b*) and (*d*) in the network diagram of Fig. 1, consists of four separate inverter units, each connected to one of the four battery strings. During the *discharging* mode, the inverters convert the DC power into 3-phase AC power. During the *charging* mode, the AC power is converted to DC. The BESS operates in three states depending on whether the battery is in *idle*, *charging* or *discharging* mode. A basic approach to consider the power losses of the energy flows during the conversion and *charging* or *discharging* processes is by incorporating an estimation of the efficiency of the power electronic devices for both the *charging* and *discharging* modes.

$$P_b^{das}(k) = \frac{1}{\eta_{ch}} \cdot P_{d,ch}^{das}(k) + \eta_{dis} \cdot P_{d,dis}^{das}(k) \qquad (2.4)$$

where n_{ch}, and n_{dis} are the efficiency factors of the inverters system during the *charging* and *discharging* modes respectively.

The charging and discharging efficiencies of a BESS are found to depend on a range of parameters such as the power rate, the temperature, the SoC and the internal resistance [28]. Since the focus of this work is not the exact modelling of the losses of the BESS, a simple representation will be used. Some preliminary analysis of the measurements from Enexis, show that both charging and discharging efficiencies can be assumed to be around 0.8. Therefore, at all the analyses in that thesis, the efficiencies are going to be considered constant and equal to 0.8.

In grid-connected applications, the output of an inverter can also inject current into the grid according to control actions (i.e., as a current source). In a current-controlled inverter the voltage and frequency are defined by the bus to which the power electronic device is connected.

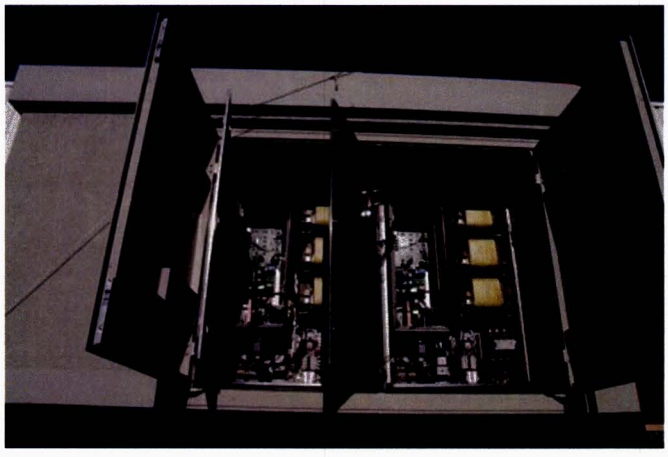

Figure 2.3 Photo of the two inverters of the BESS at Etten Leur, seen from the side-door.

2.2.1.4. The Control System

As the controller software runs on server hardware, it offers great flexibility and customization possibilities. By simply updating controller software, a different control strategy can be executed. Among other basic functionalities of the control system, the controller executes the overall control algorithm, that determines the inverter set points (these set points are sent to the inverters via a LAN connection), while there is the possibility to import external variables which might be necessary for executing the optimisation algorithm.

2.2.1.5. Costs of the BESS

The total cost of a BESS includes costs for the battery itself, the power electronics, the monitoring as well as engineering and installation costs. Table 2.2. presents the abovementioned costs for the BESS in Etten-Leur.

The engineering costs are mentioned to be relatively high. This can be explained by the pilot character of the project. When large scale deployment is applied to such battery storage systems, the engineering costs are expected to be considerably lower.

Table 2.2 Analytical and total costs of the BESS.

Description	Amount
Battery	350.000
Power electronics	150.000
Operating system	25.000
Engineering, security testing, installation	230.000
Commissioning Smart Storage	44.000
Monitoring and management (entire project duration)	108.000
Contribution of Enexis in activities of ECN	31.666
Total cost	**938.666**
Subsidy EOS Demo	365.817
Total Smart Storage (cost - subsidy)	572.849

2.2.2. The power profile

The coupling point (c) in Fig.1.1 is the point of the network where the PV installation and the households are connected. The aggregate power is denoted as P_c and refers to its *rms* value which ranges between -50 kW and 380 kW.

In order to define the power profile at the coupling point, an analysis is made for the PV generation and the household's profile. The PV profiles both for summer and winter are presented in Fig.2.4 and Fig.2.5 and are generated based on historic data from KNMI [29], for the year 2012, considering the hourly solar irradiation at Etten-Leur and taking into account the efficiency, the installation angle and the total surface of the PV panels.

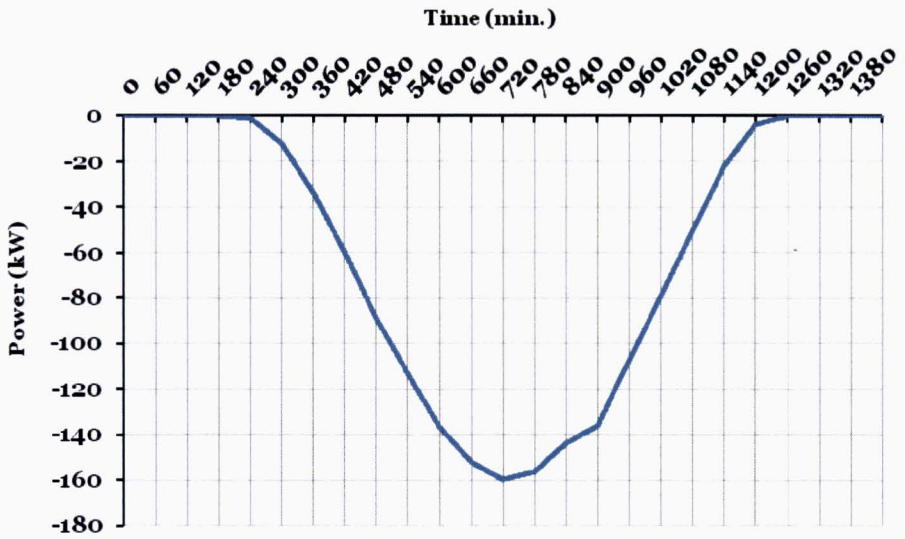

Figure 2.4 Average daily PV generation profile for the summer months.

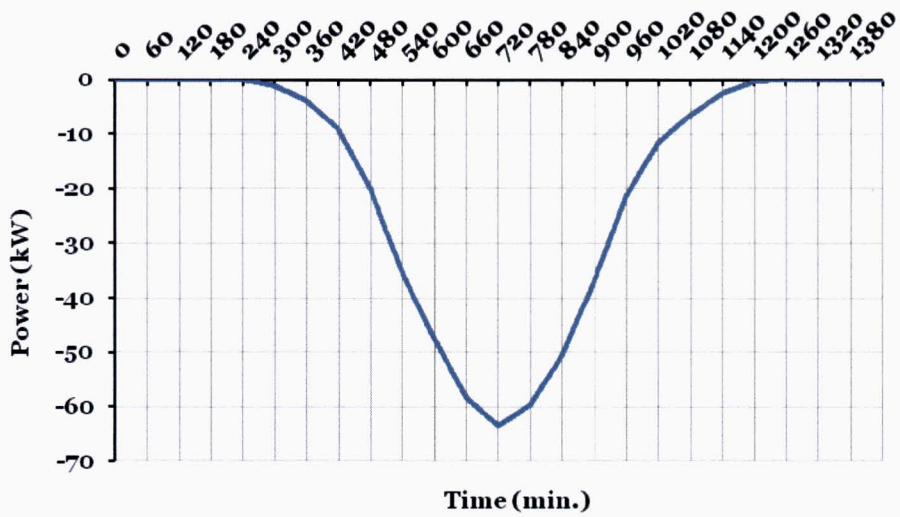

Figure 2.5 Average daily PV generation profile for the winter months.

The PV generation is depicted to be negative because as it was mentioned, power values are considered positive for energy flows from the LV busbar towards the loads and the PV panels. For energy flow from the panels to the MV bus, the power values are considered negative.

As it is expected, there is a peak at around 12h00, when the solar radiation is the highest during the day, while at the first and last hours of the day it approximately zero. At the peak of the summer profile, the power is around 160 kW, while at the winter the peak power is around 65 kW.

By processing the measurements from the substation and the inverters of the BESS (at the points (a) and (c) in Fig.2.1) it is possible to generate a profile for the total power profile at point (c). By extracting the PV power from the P_c then, the household average power profile are generated. The average household power profile is presented at Fig.2.6 for the summer months, and at Fig.2.7 for the winter months.

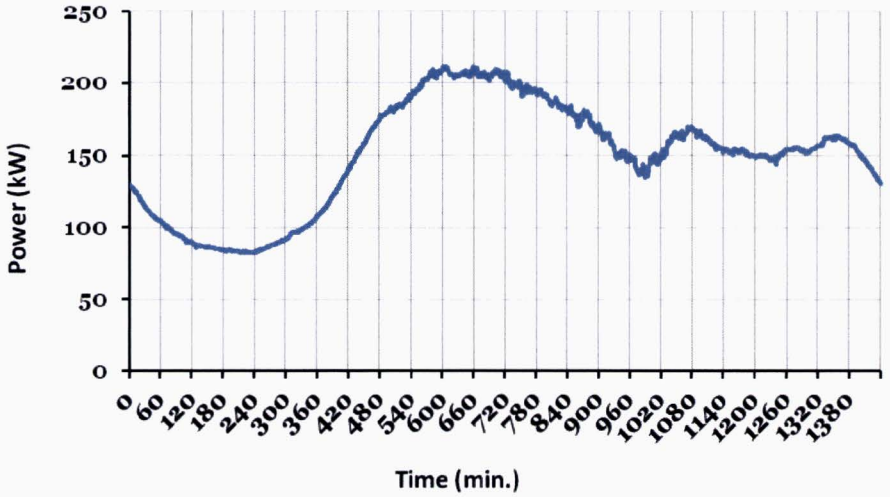

Figure 2.6 Average (summer) daily power consumption profile for the residential customers.

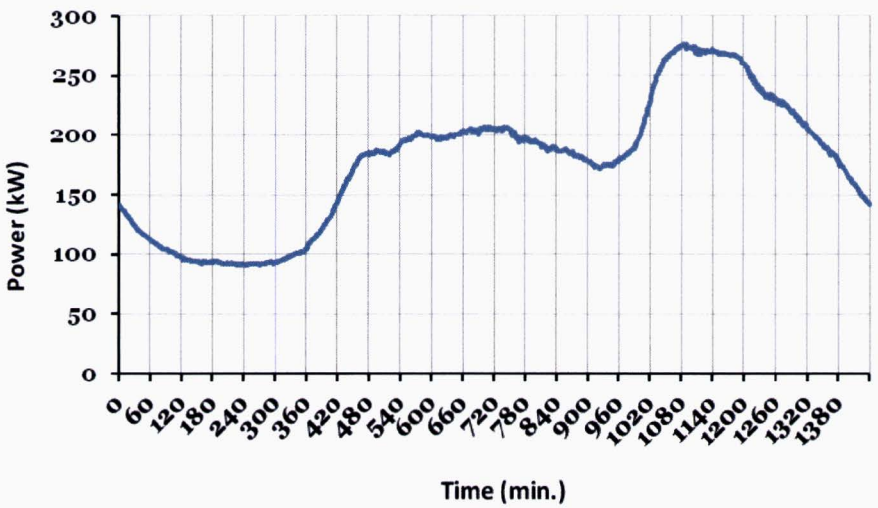

Figure 2.7 Average (winter) daily power consumption profile for the residential customers.

Both profiles are as expected, with low power consumption at the beginning and at the end of the day and larger power values at the hours from 8 a.m. to 8 p.m. In the summer profile it can be noticed that there is a peak at noon hours that could be possibly explained by cooling domestic devices i.e. air-conditioning systems. Similarly, at the winter profile there is a peak at 18-21 p.m. probably due to fact that is a time when people return home and there is increased activity in the households.

Lastly, the profiles considering the total power consumed at the coupling point (c) are generated, which are also going to be used during computer simulations in this study. The P_c summer profile is presented at Fig.2.8 whereas the P_c winter profile is presented at Fig. 2.9.

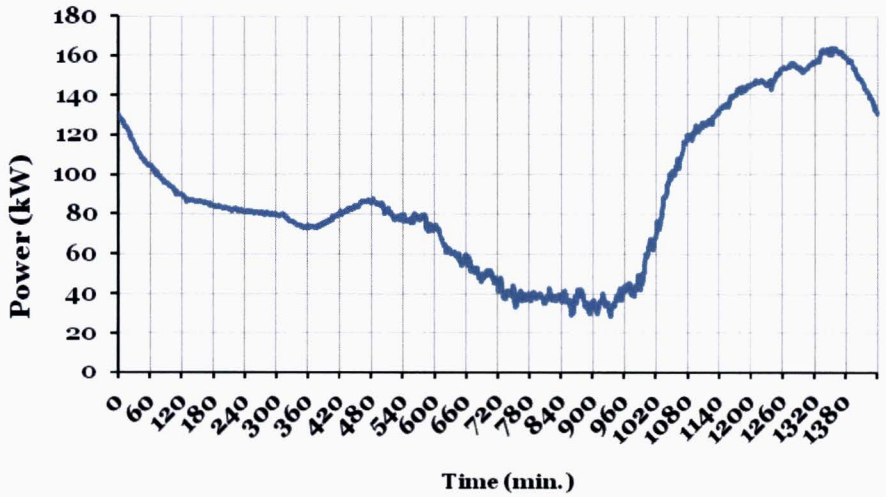

Figure 2.8 Average (summer) daily power profile at network point (c).

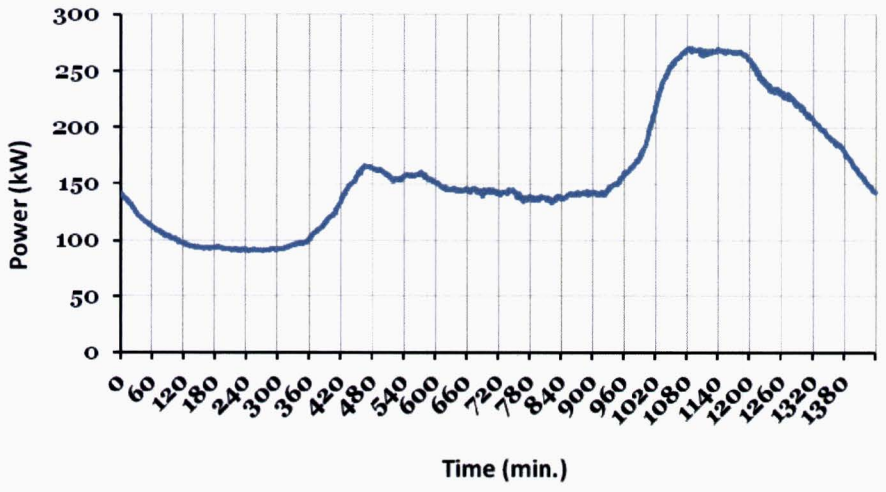

Figure 2.9 Average (winter) daily profile at network point (c).

2.3. *The Control Logic*

The goal in this work is to control the power P_b at point (b), to account for any deviations of the power P_c at point (c), to shape the exchanging power P_a with the MV grid according to (2.1). The realised power exchange P_a with the MV grid is subject to contractual agreements with electricity markets that occur prior to the real-time operations (e.g. *day-ahead*). The basic logic behind the control approach is to perform an economic optimisation which can be formulated into three control levels (i.e., upper/intermediate/lower levels).

The upper-level addresses energy trade and corresponds to discrete time periods of 1 hour, in line with the defined settlement periods for wholesale electricity trade in the APX *day-ahead* market.

The intermediate-level addresses the interaction with real-time markets for ancillary services, and specifically the balancing energy market for the provision of operating frequency restoration reserves for load frequency control which is organised by the Dutch TSO, under passive balancing. At this intermediate (intra-hour) level, the timescale corresponds to discrete time periods of 15 minutes, in line with the defined settlement periods for imbalance energy verification and settlement in the Netherlands.

The lower-level controller receives updated predictions for the power profile at the coupling point (c) (See figure 1) and the state of the system, calculates the expected future imbalances and acts accordingly (close to real-time) on a timescale of one minute.

The upper-level control problem is formulated in Chapter 3, whereas the intermediate-level control is described in Chapter 4, and finally the lower-level control problem is presented in Chapter 5.

All simulations are implemented in Matlab in a Lenovo IdeaPad Z580A with an Intel Core i5-3210M processor of 2.5 GHz with 4 GB of RAM. The optimisation problems are solved by the Global Optimisation Toolbox by using the fmincon function. The exact philosophy of the developed algorithms is provided in Appendices A and B.

2.4. State-space first order model

The state of energy (*SoE*) of a battery system at time instant k is typically expressed in a number that corresponds to a percentage and is defined as the ratio of the net amount of energy stored within the battery and the nominal capacity of the battery:

$$SoE(k) = \frac{E(k)}{E_{nom}} \tag{2.5}$$

where $E(k)$ denotes the measured energy content that is present in the battery at time instant k, and $E_{nom} = 230$ kWh refers to the nominal capacity of the battery. Since the *SoE* does not correspond to a physical quantity, it cannot be directly measured.

The most popular model-based approaches for *SoE* determination are based on state-space models that have the *SoE* as a state variable. Considering the BESS as a single input P_d={$P_{d,ch}$, $P_{d,dis}$} single output P_b system, a simplified first order linear model, in discrete-time domain, can be deduced (while assuming a *coulombic efficiency* of unity for the battery unit):

$$E(k+1) = E(k) + P_d(k) \cdot \tau \tag{2.6}$$
$$P_d(k) = P_{d,ch}(k) + P_{d,dis}(k) \tag{2.7}$$
$$P_{min} \le P_{d,dis}(k) \le 0 \tag{2.8}$$
$$0 \le P_{d,ch}(k) \le P_{max} \tag{2.9}$$
$$P_{d,ch}(k) \cdot P_{d,dis}(k) = 0 \tag{2.10}$$

The last constraint expressed in (2.10) shows that the BESS can be either in *charging* or *discharging* mode. The constraint formulated in (2.3) can be re-written as follows:

$$\begin{aligned} &\Leftrightarrow -400 \text{ kW} \le P_b(k) + P_c(k) \le 400 \text{ kW} \Leftrightarrow \\ &\Leftrightarrow -400 \text{ kW} - P_c(k) \le P_b(k) \le 400 \text{ kW} - P_c(k) \end{aligned} \tag{2.11}$$

Given the fact that $P_c(k) \in [-50, 380]$ kW, based on actual measurements, and the constraint expressed in (2.10), then (2.11) can be formulated as two inequalities:

$$\begin{aligned} &-400 \text{ kW} - P_c^{prd}(k) \le \eta_{dis} \cdot P_{d,dis}(k) \\ &\qquad \text{and} \\ &\frac{1}{\eta_{ch}} \cdot P_{d,ch}(k) \le 400 \text{ kW} - P_c^{prd}(k) \end{aligned} \tag{2.12}$$

Chapter 3 Day-ahead schedule

3.1. Day-ahead Planning

In order to assess the performance of the aggregate DR system, it is important to create a realistic representation of the aggregate residential load and PV generation in terms of energy volumes and time schedules. The aggregate power demand can be distinguished between the non-controllable part measured at network point (*c*) and the controllable part due to the power injection and absorption of the BESS which is measured at network point (*b*). Accurate short-term forecast of net generation and load is essential for the optimal real-time control of the BESS. Different techniques can be employed for creating short-term forecasts such as time series prediction methods, or artificial neural network (ANN) models such as the one presented in [30].

Since the focus of this work is not on the forecasting methods, it is assumed that a forecast of the power trajectory $P_c(k+i|k)$ is available at any time instant k, (note that in this work the power trajectory $P_c(k+i|k)$ is resembled by the actual measurements at network point (*c*)). The notation $P_c(k+i|k)$ indicates that the power predictions trajectory depends on the conditions at time instant k [31].

During the operational planning, the aggregator defines an energy schedule $P_a^{das}(h)$ for the *day-ahead* which is actually a piecewise constant function with a finite value for each settlement period of the *day-ahead* market (τ_h= 1 hour), with h=1,..., 24, whereas h=1 corresponds to the first hour of the operational day (i.e., from 00:00 to 01:00).

3.2. Day-ahead Objective Function

The *day-ahead* power schedule $P_a^{das}(h)$ is actually constructed based on: the *day-ahead* prediction of the net PV generation and residential load $P_c^{prd}(h)$, and the result of an optimisation process for the BESS which defines an optimised power profile $P_b^{das}(h)$ at network point (*b*). The *day-ahead* prediction $P_c^{prd}(h)$ is constructed based on a *day-ahead* forecast of the net PV generation and residential load (i.e., the trajectory $P_c(k-1+i|k_{ref})$ at network point (*c*), whereas for i=1 and k=1 corresponds to the first control period of the operational day and k_{ref} is the control period that signifies the gate closure time instant of the *day-ahead* market, e.g. around 12:00 of the *day-ahead*. The schedule $P_b^{das}(h)$ is actually an optimised constant power profile of the BESS for the h^{th} hour as the result of the upper-level optimisation problem which can be formulated as follows:

$$\min_{P_a(h)} \sum_{h=1}^{24} \Theta(h) \tag{3.1}$$

$$\Theta(h) = E_a^{das}(h) \cdot \pi^{prd}(h) \tag{3.2}$$

$$E_a^{das}(h) = P_a^{das}(h) \cdot \tau_h \tag{3.3}$$

$$P_a^{das}(h) = P_b^{das}(h) + P_c^{prd}(h) \tag{3.4}$$

where $\Theta(h)$ is a cost function that represents the hourly costs for purchasing an amount of electrical energy $E_a^{das}(h)$ in (Wh) at a price $\pi^{prd}(h)$ in (€/Wh) from the *day-ahead* market, whereas $P_d^{das}(h) = \{P_{d,ch}^{das}(h), P_{d,dis}^{das}(h)\}$ is the input trajectory for the BESS which satisfies the objective function and refers to the DC *charging* and *discharging* power set points. For the price values $\pi^{prd}(h)$ it is assumed that a forecast is available, resembled by the actual market clearing prices of the *day-ahead* market in the Netherlands for the year 2012 [32]. Considering that $P_c^{prd}(h)$ is considered as a known and fixed parameter, by substituting Pd from (2.4), (3.1) can be rewritten as:

$$\min_{P_d^{das}(h)} \sum_{h=1}^{24} P_b^{das}(h) \cdot \pi^{prd}(h) = \min_{P_d^{das}(h)} \sum_{h=1}^{24} \left(\frac{1}{\eta_{ch}} \cdot P_{d,ch}^{das}(h) + \eta_{dis} \cdot P_{d,dis}^{das}(h)\right) \cdot \pi^{prd}(h) \tag{3.5}$$

Subject to the *day-ahead* constraints:

$$P_{min} \le P_{d,dis}^{das}(h) \le 0, \quad h \in [1,24] \tag{3.6}$$

$$0 \le P_{d,ch}^{das}(h) \le P_{max}, \quad h \in [1,24] \tag{3.7}$$

$$P_{d,ch}^{das}(h) \cdot P_{d,dis}^{das}(h) = 0 \tag{3.8}$$

$$SoE_{min}^{das} \le SoE^{das}(h+1) \le SoE_{max}^{das} \tag{3.9}$$

$$-400 \text{ kW} - P_c^{prd}(h) \le \eta_{dis} \cdot P_{d,dis}^{das}(h) \quad \text{and} \quad \frac{1}{\eta_{ch}} \cdot P_{d,ch}^{das}(h) \le 400 \text{ kW} - P_c^{prd}(h) \tag{3.10}$$

where $P_{min} = -400$ kW, $P_{max} = 100$ kW. In the above mentioned constraints, it could also be added one to ensure that the SoE at the beginning and at the end of each day remains the same. Nevertheless, the battery always respects this constraint by the default definition of the day-ahead optimization and during a day, the sum of all charging power set points is equal to the sum of all discharging setpoints.

The results of the *day-ahead* optimisation problem are optimised *charging* and *discharging* profiles of the BESS, i.e., hourly power set-point values $P_d^{das}(h) = \{P_{d,ch}^{das}(h), P_{d,dis}^{das}(h)\}$ and energy states $SoE^{das}(h+1)$ for h=1,..., 24. These results can be further employed in the intra-hour optimisation problem (See chapter 4).

3.3. Results of the day-ahead optimization

Given the fact that energy arbitrage applications through storage technologies are susceptible to the efficiency of the storage systems, the basic principle behind the decision whether the battery should be used or not in a specific day is dependent on the term $\pi_{\max} \cdot n_{dis} - \frac{\pi_{\min}}{n_{ch}}$ where $\pi_{\max}$ is the highest price of the day-ahead market and $\pi_{\min}$ the lowest.

If this term is positive, then the battery will be charged at the hour when the price is $\pi_{\min}$ and discharged when the price is $\pi_{\max}$. Accordingly, the algorithm continues comparing the next highest price with the next lowest and if the term mentioned above is positive and subject to the *SoE* constraints, then another charging and discharging cycle is scheduled.

Practically, the above-mentioned term is representing the losses of the system, and therefore determines the decision whether the battery should or not be charged or discharged at a specific time instant (i.e. at the h^{th} hour).

As it is already mentioned, the charging and discharging efficiencies for the investigated BESS at Etten-Leur were estimated to be around 0.8 based on actual measurements, and for this investigation are assumed to be constant.

An example of the day-ahead optimization is provided in Figure 3.1 where the charging and discharging profiles are illustrated for a random day of 2012 based on the APX day ahead clearing prices.

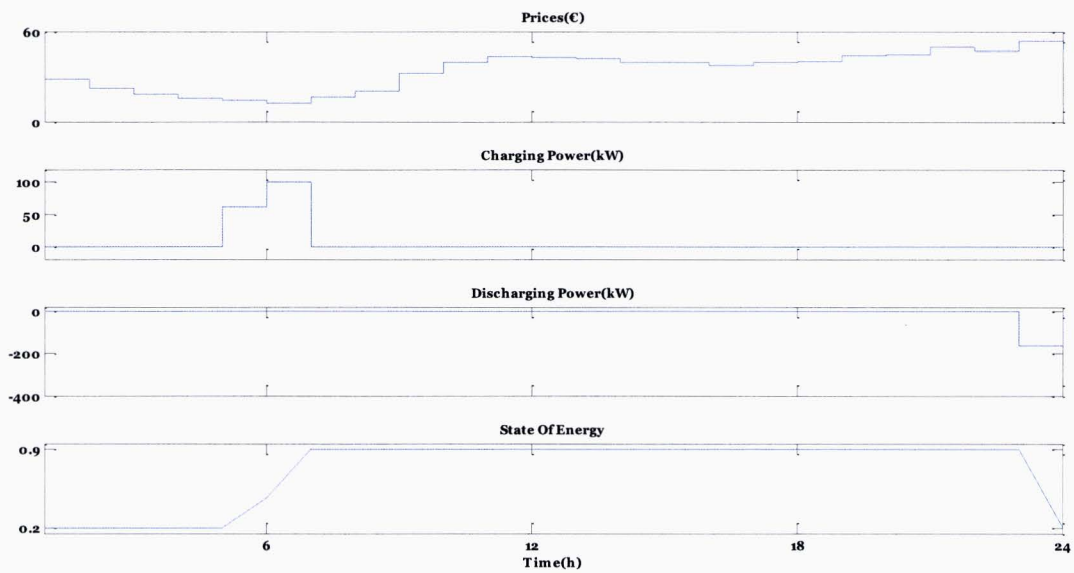

Figure 3.1 Typical BESS optimisation. APX prices for the 9th June, 2012.

As can been seen in Figure 3.1., at the lowest price during the day the BESS is charged until it reaches its maximum allowed SoE. As it cannot reach it within one hour, due to maximum allowed charging power (100 kW), the charging takes place at the two hours with the lowest price (5th and 6th). As it is expected, the battery is discharged at the time with the highest price, which happens to be the 24th hour for that day.

A typical day ahead optimised profile for the investigated BESS is depicted in Figure 3.1. However, depending on the expected prices and considered efficiencies the optimised profile can be characterised by more than one charging and discharging cycle. An example where the battery is charged and discharged twice during one day is provided in Figure 3.2. based on prices from the 7th of February, 2012.

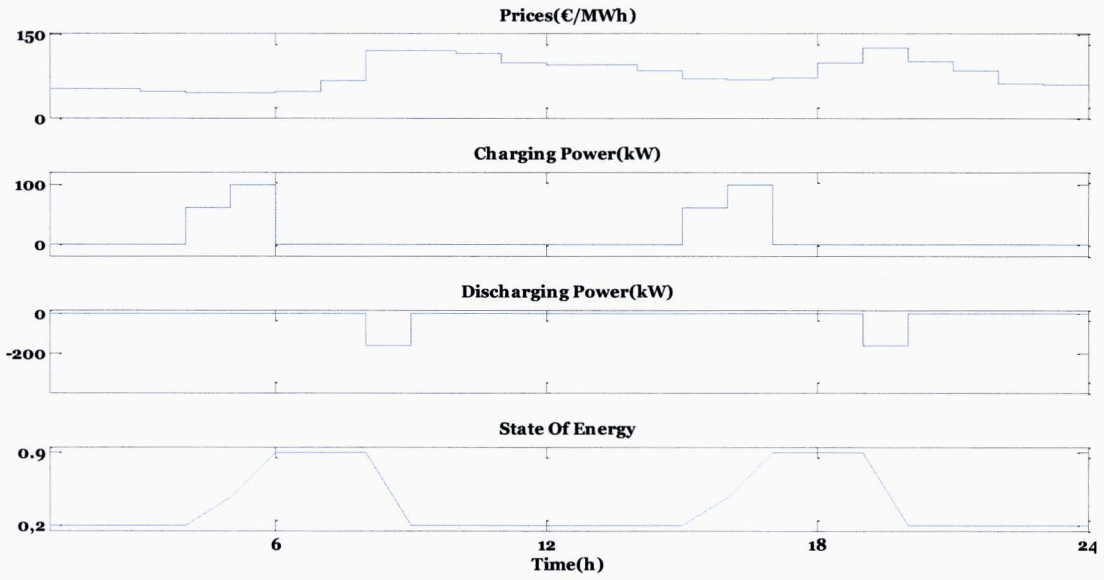

Figure 3.2 Optimal BESS optimisation with two charging and discharging cycles during one day (APX prices from February 7, 2012).

Another distinct case during the day-ahead optimisation is when the expected prices and considered efficiencies result in a null schedule for charging and discharging. An example with such a profile is provided in Figure 3.3.

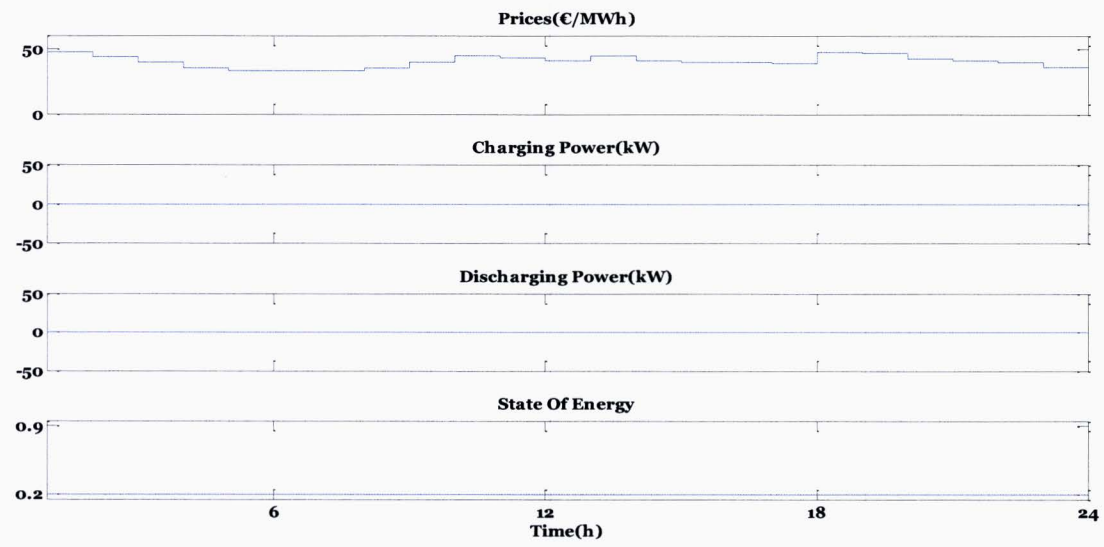

Figure 3.3 BESS optimisation with no optimised charging and discharging profiles (APX prices from the 21st January, 2012).

Focusing on data for the year 2012, the revenues that the BESS can generate under the defined day ahead optimisation are on average around 5€ per day. This amount may increase to 27.5€ for the investigated BESS for a selected day and theoretically can reach up to 36€ for an ideal system which is characterised by no energy losses.

To provide an impression of the potential revenues from energy arbitrage application, and how these revenues vary depending on the efficiencies of the BESS and the expected day-ahead prices, a representative sample of results is provided in tables 3.1 and 3.2. Specifically, three cases are considered: case 1 stands for charging and discharging efficiencies equal to 0.8, case 2 stands for charging and discharging efficiencies equal to 0.9, and case 3 stands for charging and discharging efficiencies equal to 1. Furthermore, a selection of days from the year 2012 that are characterised by large price differences and two daily charging and discharging cycles are included in Table 3.1. whereas days characterised by average daily price differences are included in Table 3.2.

Table 3.1 Daily revenues for the potentially most profitable days for the year 2012 based on APX data.

Day	Revenues (€) Case 1	Revenues (€) Case 2	Revenues (€) Case 3
06/02	10.8	17.6	23.8
08/02	18.5	27.5	36.4
09/02	13.3	19.7	27.9
10/02	11.6	18	24.1

Table 3.2 Daily revenues for the average days.

Day	Revenues (€) Case 1	Revenues (€) Case 2	Revenues (€) Case 3
23/02	4.1	7.7	11.6
09/06	4.3	5.5	7.7
05/10	3.8	5.9	9.6
18/12	3.6	5.8	9

3.4. Economic results of the day-ahead optimisation

Based on computer simulation for the years from 2000 to 2012, large deviations in calculated annual revenues can be observed. The results from computations are presented in Tables 3.3 and 3.4. The first table captures the annual profits per year and for several charging and discharging efficiencies between 0.5 and 1 while the second table presents the percentage of the days of the whole year that the BESS is being used for the considered years and BESS efficiencies.

Table 3.3 Calculated profits per year for the period 2000-2012 for varying charging and discharging efficiencies.

	Annual Profits (€)					
	0.5	**0.6**	**0.7**	**0.8**	**0.9**	**1**
2012	34	141	489	1170	1904	3128
2011	33.8	106.7	289.7	698.5	1417	2581
2010	45	132	383	938	1596	2573
2009	153.7	406	858	1385	2015	2964
2008	285	764	1615	2602	3697	5406
2007	754	1374	2112	2865	3735	4890
2006	1358	2294	3393	4489	5730	7440
2005	1277	2055	3025	4089	5271	6832
2004	685	1151	1729	2356	3008	3875
2003	3143	4269	5601	6992	8526	10325
2002	1626	2264	2936	3679	4540	5671
2001	1853	2614	3464	4389	5485	6853
2000	2125	3018	3949	5104	6333	7760

Table 3.4 Calculated percentage of the days of a whole year that the day-ahead optimization is performed.

	Percentage of days used (%)					
	0.5	**0.6**	**0.7**	**0.8**	**0.9**	**1**
2012	8.2	26.8	65.6	97.5	100	100
2011	7.7	16.7	37.3	82.7	99.5	100
2010	12.1	24.7	65.5	97.3	100	100
2009	30.7	65.7	90	99.2	100	100
2008	28.7	58.5	88.5	99.5	100	100
2007	55.6	84.9	97.5	100	100	100
2006	60.5	91.8	99.7	100	100	100
2005	40.3	64.1	92.6	100	100	100
2004	47.5	71.5	93.8	99.7	100	100
2003	71.5	93.4	99.5	100	100	100
2002	76.7	92	99.2	100	100	100
2001	59.2	83.6	97.8	100	100	100
2000	28.7	31.9	51.6	71.3	76.8	100

By processing the data from APX for the period 2000-2012, large prices deviations can be noticed during a day between several years. It is mentioned above, that the term that mostly affects the annual revenues is the difference between the highest and lowest price of the day-ahead market. To assist in interpreting the results, the historical price volatility metric is utilised in the study.

3.5. Historical volatility

3.5.1. Definition of the historical volatility

In finance, volatility is a measure for variation of price of a financial instrument over time. Historic volatility is derived from time series of post market prices. In competitive electricity markets, prices are not regulated any longer, but are determined by the market operators for each specific interval of the day (e.g. every 1 hour or 15 min), while taking into account various economic and operational factors. Given the uncertainty associated with the electricity market prices, and such a wide variety of options, the applications of volatility analysis to competitive electricity markets are undoubtedly useful for market participants [33].

Historical volatility is defined as the standard deviation of arithmetic or logarithmic returns over a time window T. The logarithmic return, over the time period h, is defined as follows:

$$r_{t,h} = \ln\left(\frac{p_t}{p_{t-h}}\right) = \ln(p_t) - \ln(p_{t-h})$$

where p_t denotes the spot price for a commodity at time t.

The arithmetic return, over the time period h, is defined as

$$R_{t,h} = \frac{p_t - p_{t-h}}{p_{t-h}}$$

The estimated value of historical volatility over the time window T can be calculated as [33]:

$$\sigma_{h,T} = \sqrt{\frac{\sum_{t=1}^{N_o}\left(r_{t,h} - \bar{r}_{h,T}\right)^2}{N_o - 1}}$$

where $\sigma_{h,T}$ is the estimated value of historical volatility, N_o is the number of $r_{t,h}$ observations, $\bar{r}_{t,h}$ is the average of the returns $r_{t,h}$ (either logarithmic or arithmetic) , all of them for the time window T.

In this volatility analysis study, $h = 1$ $(hour)$ which is the settlement period for the day-ahead spot market for electricity.

The time window is one day, as the scope of this analysis is to compute the daily volatilities, based on both logarithmic and arithmetic returns for each year and compare them with each other. Therefore, T is defined as $T = 1$ (day) and $N_o = 24$.

3.5.2. Historical price volatility calculations

Figure 3.5 depicts the annual revenues for the years 2000-2012, assuming charging and discharging efficiencies equal to 0.8. Figures 3.6 and 3.7 show the boxplots of the historical price volatilities for the same years, based on arithmetic and logarithmic returns calculations respectively. Each boxplot depicts all the daily volatilities for a year and the spacing between the different parts of the box help indicate the degree of spreading and identify the outliers. On each box, the red central mark is the median, the edges of the blue box are the 25th and 75th percentiles, the whiskers extend to the most extreme data points not considered outliers, and outliers (i.e. observations that are numerically distant from the rest of the data) are plotted individually.

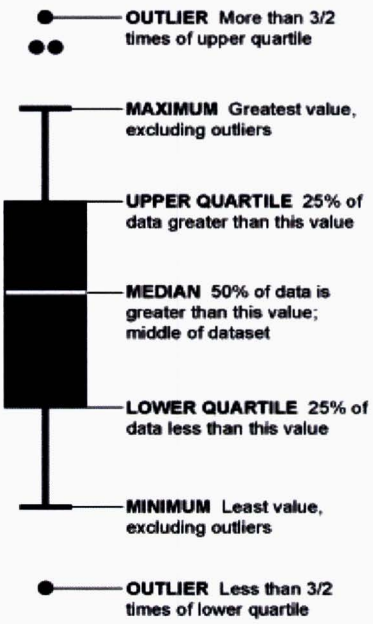

Figure 3.4 Description of the boxplots used for volatility analysis[2].

[2] http://www.mathworks.com/help/symbolic/mupad_ref/plot-boxplot.html

The results of the volatility calculations for the years 2000-2012 are shown at the figures below:

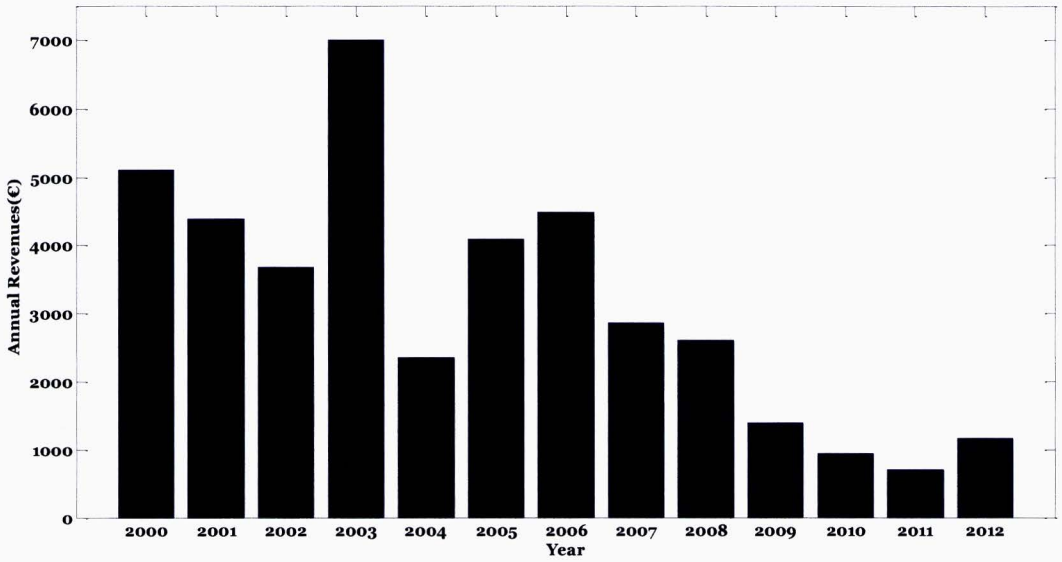

Figure 3.5 Annual revenues per year from the day-ahead optimisation (charging and discharging efficiencies are considered to be 0.8).

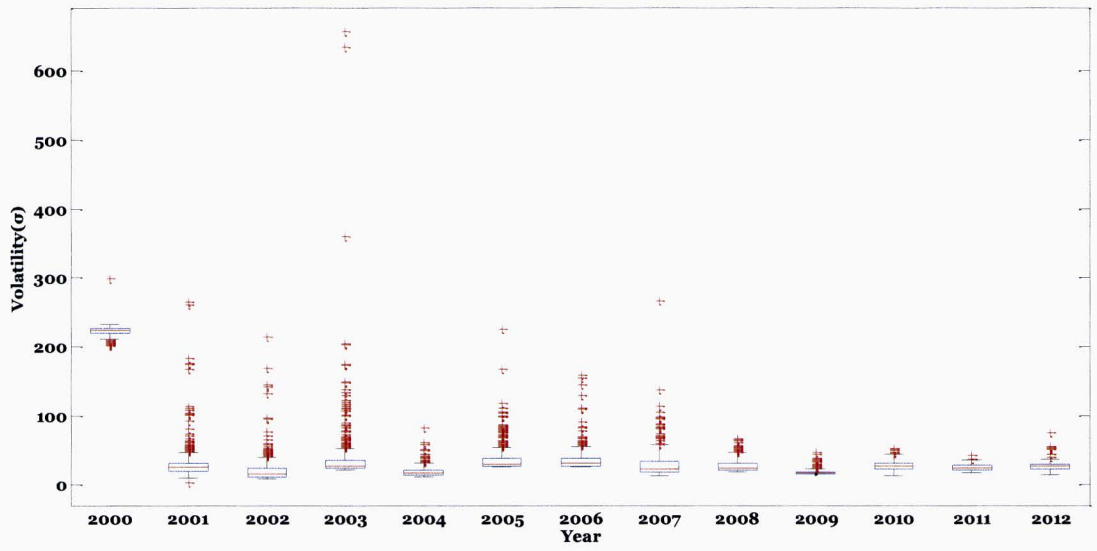

Figure 3.6 Boxplot of historical price volatilities per year based on calculations of the arithmetic return.

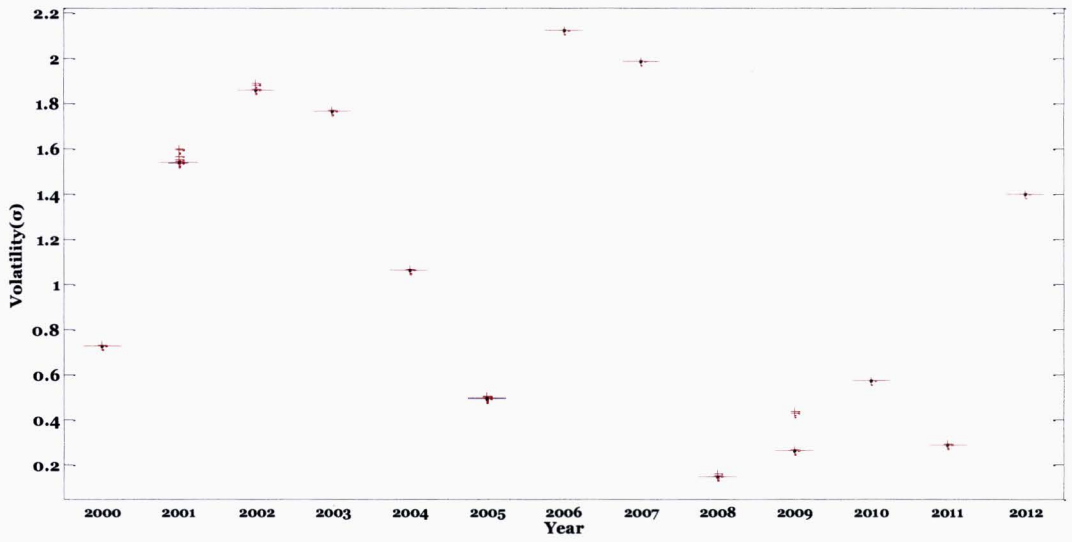

Figure 3.7 Boxplot of historical price volatilities per year based on the calculations of the logarithmic return.

Based on observations and comparisons between figures 3.4 - 3.6, it can be noticed that the arithmetic volatility seems to be rather correlated with revenues while the logarithmic is not. The correlation of the profits with either the median values or the whole box containing the 50% of the data is low for both arithmetic and logarithmic volatilities. However, in the case of the arithmetic volatility, it appears that the outliers and the profits are well correlated. It can be concluded, that the annual revenues are mostly related to the magnitude and the frequency of the outliers above the upper quartile.

This volatility analysis explains up to a point the correlation of the annual profits with the volatility of the prices. However, the definition of historical volatility is based on the assumption that the logarithmic returns follow an independent and identically distributed random variable which means that they are assumed to have a random behavior but with constant mean and variance over the time window T. However, electricity prices are characterized by a seasonal behavior depending on the specific day, week or season of the year and therefore could not be seen as independent and identically distributed random variables [33].

Apart from that, it is not only the price differences during a day that define the annual profits. The SoE of the BESS at a certain time instant is a factor that also affects the scheduling of the charging/discharging cycles regardless of the prices mentioned. This dependence though, cannot be captured by the analysis of the historical prices volatility.

Chapter 4 Intra-hour Schedule

4.1. Intra-hour Planning

Following the clearing of the *day-ahead* market, the aggregator has defined an hourly power schedule $P_a^{das}(h)$ for the *day-ahead* which is actually a piecewise constant function with a finite power value for each hour h of the operational day, h=1,..., 24. The verification of the energy provision and the financial settlement by the system and market operators are performed *a posteriori*, i.e., after the operational day, and is performed on the basis of settlement periods τ_s of 15 minutes each. Therefore, the hourly power schedule $P_a^{das}(h)$ for the *day-ahead* is transformed on the basis of 15 min., i.e., $P_a^{das}(l)$, with l=1,..., 96. Any energy imbalance $\Delta E_a(l)$ with respect to the energy schedule $P_a^{das}(l)$ must be internally solved by the aggregator before the end of the l^{th} settlement period, or settled with the TSO through the imbalance settlement.

Moving closer to the operational day, updated forecasts are at the disposal of the aggregator which can be further employed during intra-hour optimisation. Taking the Dutch market design as a reference, the aggregator can contribute to system balancing through passive contribution. Passive contribution can only be identified in case of unidirectional dispatch during a settlement period (i.e., when the system state is: '1' or '−1'). Therefore, if the system is expected to be *short* or *long* during certain settlement periods, then the aggregator can decide to maintain an amount of internal imbalance which can be regarded as passive contribution and allow for additional revenues. An analysis of the data for the year 2012, indicate that the Dutch system was either in *short* or *long* position for about 81.5 % of the time [24].

At the end of the *operational planning* day, the operations proceed with the *intra-hour* planning which occurs for each l^{th} settlement period. At current settlement period q, the aggregator creates an updated forecast about the net PV generation and residential load, i.e., $P_c^{prd}(q+m \mid q)$, with $m=1,\ldots,48$. At the same time instant the aggregator generates a prediction about the system state and imbalance prices for the forthcoming settlement periods. Let us denote the predicted imbalance prices as $\pi_{surpl}^{prd}(q+m \mid q)$ and $\pi_{short}^{prd}(q+m \mid q)$ for net energy *surplus* and *shortage* respectively, and the predicted system state $s^{prd}(q+m \mid q)$, with $m=1,\ldots,48$.

Based on (2.4), from the optimised charging profiles $P_d^{das}(h)$, the $P_b^{das}(l)$ profiles can be defined. During the *intra-hour* scheduling the expected energy imbalance $\Delta E_{imb}^{prd}(l)$ for the lth settlement period can be expressed as follows:

$$\Delta E_{imb}^{prd}(l) = (P_a^{das}(l) - P_b^{ihs}(l) - P_c^{ihs}(l)) \cdot \tau_s \qquad (4.1)$$

where the *intra-hour* power schedule $P_b^{ihs}(l) = P_b^{das}(l) + dP_b^{ihs}(l)$, and $dP_b^{ihs}(l)$ is a deviation value which can be set to command for corrective actions with reference to the *day-ahead* optimised charging schedule $P_b^{das}(l)$. Equivalently, $P_c^{ihs}(l) = P_c^{das}(l) + dP_c^{ihs}(l)$, where $P_c^{ihs}(l)$ is the most recent prediction of the net generation and load at network point (c), and $dP_c^{ihs}(l) = 0$ when assuming a prediction with no errors.

4.2. Intra-hour Optimisation

Considering the current settlement period q, the objective function for the *intra-hour* optimisation problem can be formulated as a profit function $\Pi(q+m\,|\,q)$ that represents the profits associated with the passive contribution in the real-time balancing market for the $(q+m)^{\text{th}}$ settlement period, with $m=1,\ldots,48$. The optimisation objective is to maximise the objective function:

$$\max_{dP_d^{ihs}(q+m|q)} \sum_{m=1}^{48} \Pi(q+m\,|\,q) \tag{4.2}$$

$$\Pi(q+m\,|\,q) = \Delta E_{imb}^{prd}(q+m\,|\,q)\cdot \pi_{imb}^{prd}(q+m\,|\,q) \tag{4.3}$$

$$\Delta E_{imb}^{prd}(q+m\,|\,q) = (-dP_b^{ihs}(q+m\,|\,q) - dP_c^{ihs}(q+m\,|\,q))\cdot \tau_s \tag{4.4}$$

where $\pi_{imb}^{prd}(q+m\,|\,q)$ is the predicted imbalance price in (€/MWh) for the real-time balancing market and $dP_d^{ihs}(q+m\,|\,q)$ is the input trajectory which satisfies the objective function and refers to a DC *charging* (and *discharging*) power deviation value. The latter can be expressed according to the following equation:

$$dP_b^{ihs}(l) = \frac{1}{\eta_{ch}}\cdot dP_{d,ch}^{ihs}(l) + \eta_{dis}\cdot dP_{d,dis}^{ihs}(l)\,. \tag{4.5}$$

Note that the price $\pi_{imb}^{prd}(l)$ is dependent of the sign of the net energy imbalance $\Delta E_{imb}^{prd}(q+m\,|\,q)$. Therefore, $\pi_{imb}^{prd}(l) = \{\pi_{surpl}^{prd}(l), \pi_{short}^{prd}(l)\}$ depending on whether there is energy *surplus* $(\Delta E_{surpl}^{prd}(l) \geq 0)$ or *shortage* $(\Delta E_{short}^{prd}(l) \leq 0)$.

For the price values $\pi_{imb}^{prd}(l)$ it is assumed that a forecast is available, resembled by the actual market prices of the real-time balancing market in the Netherlands for the year 2012 [26].

The resulted hourly charging states of the *day-ahead* optimisation problem $SoE^{das}(h)$, for h=1,..., 24, are transformed on a 15 min. basis by using (4.6):

$$SoE_{ref}^{ihs}(l) = SoE^{das}(h) + \frac{SoE^{das}(h+1) - SoE^{das}(h)}{4}\cdot(l-1-4\cdot(h-1)) \tag{4.6}$$

where $l \in [4\cdot(h-1)+1, 4\cdot h]$ for each hour h, whereas l=1, ..., 96.

subject to the *intra-hour* constraints:

$$P_{min} \le P_{d,dis}^{das}(l) + dP_{d,dis}^{ihs}(l) \le 0 \tag{4.7}$$

$$0 \le P_{d,ch}^{das}(l) + dP_{d,ch}^{ihs}(l) \le P_{max} \tag{4.8}$$

$$P_{d,ch}^{ihs}(l) \cdot P_{d,dis}^{ihs}(l) = 0 \tag{4.9}$$

$$SoE_{min} \le SoE_{mpc}^{ihs}(l+1) \le SoE_{max} \tag{4.10}$$

$$SoE^{ihs}(q+48) = SoE_{ref}^{ihs}(q+48) \tag{4.11}$$

$$-400 \text{ kW} - P_c^{prd}(l) \le \eta_{dis} \cdot P_{d,dis}^{ihs}(l) \quad \text{and} \quad \frac{1}{\eta_{ch}} \cdot P_{d,ch}^{ihs}(l) \le 400 \text{ kW} - P_c^{prd}(l) \tag{4.12}$$

where (4.11) reflects the fact that during the intra-hour optimisation, the charging state at the end of the prediction horizon should meet the reference value of the *day-ahead* optimisation.

The imbalance prices for shortage and surplus given by Tennet and presented at Table 2.2. consider the active balancing market. As passive contribution refers only to the cases when the system state in a settlement period is 1 or -1, the prices have to be defined appropriately to match the objective function. The imbalance prices have to be defined in a way, such that the term of the objective function $\Pi(q+m \mid q) = \Delta E_{imb}^{prd}(q+m \mid q) \cdot \pi_{imb}^{prd}(q+m \mid q)$ is positive when the aggregator is receiving additional revenues from passive balancing and it is negative when the aggregator is facing penalties. The appropriate definition of the imbalance prices is given in Table 4.1.

Table 4.1 Intra-hour optimisation pseudo code: imbalance prices definition.

1.	**begin**;
2.	# Current settlement period is q (e.g., the last settlement period of the *operational planning day*), whereas τ_s = 15 min., m= 1, ..., 48.
3.	**for** m = 1 to 48 **do**
4.	**if** $s^{prd}(q+m) = 0$ **then**
5.	**if** $\Delta E_{imb}^{prd}(q+m) > 0$ **then**
6.	$\pi_{imb}^{prd}(q+m) = \pi_{surpl}^{prd}(q+m) = -\text{abs}(\pi_{mid}^{prd}(q+m) - \pi_{ic}^{prd}(q+m))$ **else**
7.	**if** $\Delta E_{imb}^{prd}(q+m) < 0$ **then**
8.	$\pi_{imb}^{prd}(q+m) = \pi_{short}^{prd}(q+m) = \text{abs}(\pi_{mid}^{prd}(q+m) + \pi_{ic}^{prd}(q+m))$
9.	**end if**
10.	**if** $s^{prd}(q+m) = 2$ **then**

11. **if** $\Delta E_{imb}^{prd}(q+m)>0$ **then**

12. $\pi_{imb}^{prd}(q+m)=\pi_{surpl}^{prd}(q+m)=-\text{abs}(\pi_{-}^{prd}(q+m)-\pi_{ic}^{prd}(q+m))$ **else**

13. **if** $\Delta E_{imb}^{prd}(q+m)<0$ **then**

14. **If** (emergency power is called) **then**

15. $\pi_{imb}^{prd}(q+m)=\pi_{short}^{prd}(q+m)=\text{abs}(\max(\pi_{+}^{prd}(q+m),\pi_{em}^{prd}(q+m))+\pi_{ic}^{prd}(q+m))$

16. **else** $\pi_{imb}^{prd}(q+m)=\pi_{short}^{prd}(q+m)=\text{abs}(\pi_{+}^{prd}(q+m)+\pi_{ic}^{prd}(q+m))$

17. **End if**

18. **end if**

19. **if** $s^{prd}(q+m)=-1$ **then**

20. **if** $\Delta E_{imb}^{prd}(q+m)>0$ **then**

21. $\pi_{imb}^{prd}(q+m)=\pi_{surpl}^{prd}(q+m)=\pi_{-}^{prd}(q+m)-\pi_{ic}^{prd}(q+m)$ **else**

22. **if** $\Delta E_{imb}^{prd}(q+m)<0$ **then**

23. $\pi_{imb}^{prd}(q+m)=\pi_{short}^{prd}(q+m)=\pi_{-}^{prd}(q+m)+\pi_{ic}^{prd}(q+m)$ **else**

24. **end if**

25. **if** $s^{prd}(q+m)=+1$ **then**

26. **if** $\Delta E_{imb}^{prd}(q+m)>0$ **then**

27. **if** (emergency power is called) **then**

28. $\pi_{imb}^{prd}(q+m)=\pi_{surpl}^{prd}(q+m)=\max(\pi_{+}^{prd}(q+m),\pi_{em}^{prd}(q+m))-\pi_{ic}^{prd}(q+m)$

29. **else** $\pi_{imb}^{prd}(q+m)=\pi_{surpl}^{prd}(q+m)=\pi_{+}^{prd}(q+m)-\pi_{ic}^{prd}(q+m)$

30. **End if**

31. **if** $\Delta E_{imb}^{prd}(q+m)<0$ **then**

32. **if** (emergency power is called) **then**

33. $\pi_{imb}^{prd}(q+m)=\pi_{short}^{prd}(q+m)=\max(\pi_{+}^{prd}(q+m),\pi_{em}^{prd}(q+m))+\pi_{ic}^{prd}(q+m)$

34. **else** $\pi_{imb}^{prd}(q+m)=\pi_{surpl}^{prd}(q+m)=\pi_{+}^{prd}(q+m)+\pi_{ic}^{prd}(q+m)$

35. **End if**

36. **end if**

37. **end for**

38. # The iteration continues with the next settlement period and the whole process is repeated.

39. $q = q+1$

40. **end**

As it has already been stated, the electricity prices for the imbalance market are only known ex-post and not close to real-time. Therefore, an optimisation approach that is applied just before the beginning of the PTU can only rely on a price forecasting method. It is expected that the appliance of forecasting tools, poses risks in the problem associated with erroneous predictions. Since the development of price forecasting is not the contribution of this thesis though, the price prediction is going to be considered perfect (by utilising the actual historical market data) and only in some case studies discussed in section 4.3. specific prediction errors for the state of the system and the power imbalance at point (c) are considered. Aspects concerning the risks that are imposed in the system from the presence of the forecasting tools are not addressed at all throughout this thesis.

4.3. Results of the intra-hour optimisation

The results of the *intra-hour* optimisation problem are optimized *charging* and *discharging* profiles of the BESS, i.e., power set-point values $dP_d^{ihs}(l) = \left\{dP_{d,ch}^{ihs}(l), dP_{d,dis}^{ihs}(l)\right\}$ and charging states $SoE_{ref}^{ihs}(l+1)$ for an horizon of 48 PTUs starting from the current PTU. The results about the charging states will be further employed in the real-time optimisation problem.

An example of the intra-hour optimisation is provided in Figure 4.1. where the optimised profile of the BESS is illustrated for the 7th of July, 2012 starting from the 1st PTU based on the Tennet energy imbalance prices.

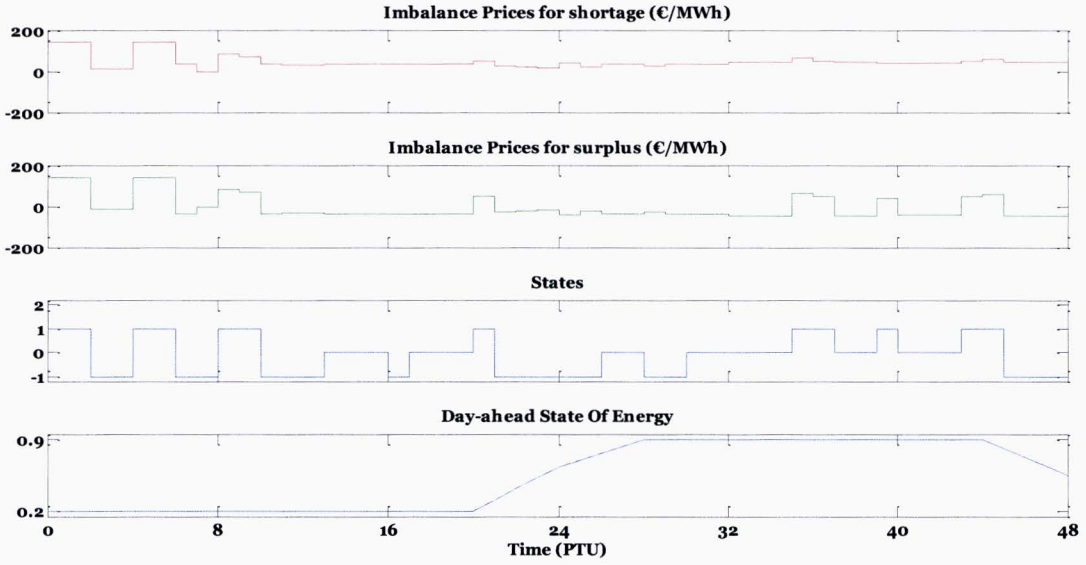

Figure 4.1 Input parameters of the intra-hour optimisation problem (An example based on TenneT data for the 7th July).

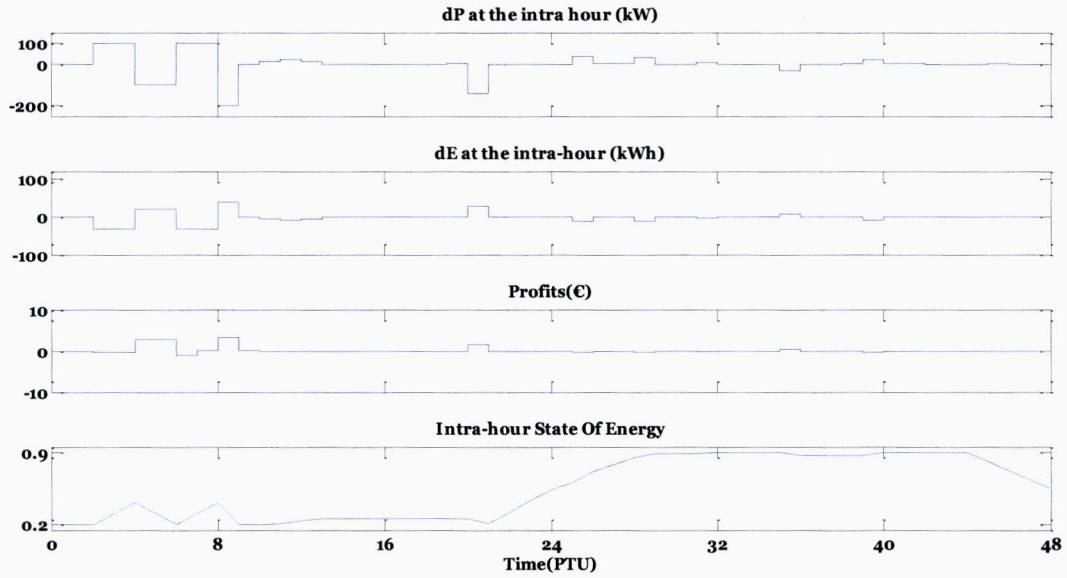

Figure 4.2 Illustration of the outputs of the intra-hour optimisation (An example based on TenneT data for the 7th July).

Figure 4.1 shows the predicted imbalance prices for surplus and shortage, the predicted state of the system and the day-ahead SoE while Fig.4.2 shows the battery optimized schedule for the horizon of the 48 PTUs, the accumulated profits per PTU, as well as the *SoE* of the BESS per PTU based on the intra-hour optimisation.

At the first 2 PTUs, the state of the system is 1. This means upwards regulation and the aggregator has an interest to maintain a positive energy imbalance ($dE > 0$). The only way that the battery system can respond to this is by being discharged. It can be observed though, that at the same time the *SoE* of the battery is at the minimum allowed bound (0.2) and therefore the battery cannot be discharged further.

At the next PTUs (3rd and 4th), the predicted state of the system changes from 1 to -1. This means downwards regulation ($dE < 0$) and the aggregator is now incentivised to maintain a negative imbalance. It can be seen that the battery reacts accordingly, by being charged with the maximum allowed power rate (100kW).

The same pattern is being followed during the whole horizon of the optimization. It can also be noticed that when the system state is either 0 or 2, the battery is neither charged nor discharged. This is expected because, as it has been stated, at the passive balancing any energy imbalance dE is going to be penalised and lead to economic losses.

In real-time operations, the intra-hour optimisation is applied at the last minute before the beginning of each PTU. The first step of this optimisation is applied at that PTU whereas at the following PTU a new optimized schedule is generated by the algorithm taking into account the updated predictions. This technique, where the prediction horizon is continuously being shifted forward, is called the receding horizon technique.

The simulations for the intra-hour optimization problem lasted on average 18 seconds with respect to the utilized hardware and software that was mentioned in Chapter 2. Therefore, the calculations for the intra-hour optimisation are performed fast enough to be implemented at the last minute of each PTU and close to real-time operations.

4.4. Case studies with erroneous predictions in the states of the system and the power profile

In real life applications, the predictions of the state of the system and the P_c power profiles are expected to involve errors and deviations from the forecasted values will most probably occur during a day. In order to ensure that the output of the optimization algorithms in such cases can account for such prediction errors, the algorithms are examined in several case studies.

In these case studies, the prediction error that is assumed to appear, considers only the state of the system at the first PTU and the power profile at the coupling network point (c).

Apart from that and in order to have a better insight of the way that a prediction error in the P_c power profile affects the whole system, the case studies are examined for both large and small errors.

The measure that is used to quantify the difference between the P_c predicted values and the P_c measurements is the Root Means Square Error (RMSE). The RMSE serves to aggregate the magnitudes of the errors in predictions into a single measure of predictive power.

The RMSE is given by

$$RMSE = \sqrt{\frac{1}{n} \cdot \sum_{i=1}^{n} (\hat{Y}_i - Y_i)^2}$$

where $\hat{Y}$ is a vector of n predictions, and Y is the vector of the measured values. In this thesis, all case studies are going to consider a large prediction error for P_c (RMSE=40) and a small prediction error (RMSE=20).

Apart from that, two different situations are considered for the forecasting of the P_c profile.

The first one, is assumed to happen in the summer and considers the case in which the PV generation is larger than predicted during the day, due to more solar irradiation, which results in a lower P_c than expected ($dP_c < 0$).

The summer case study is performed based on data from measurements at point (a) and point (c) from the 30th June 2012 and the PV forecasted and real power profiles are presented in Fig.4.3 and Fig.4.4 for small and large prediction error respectively.

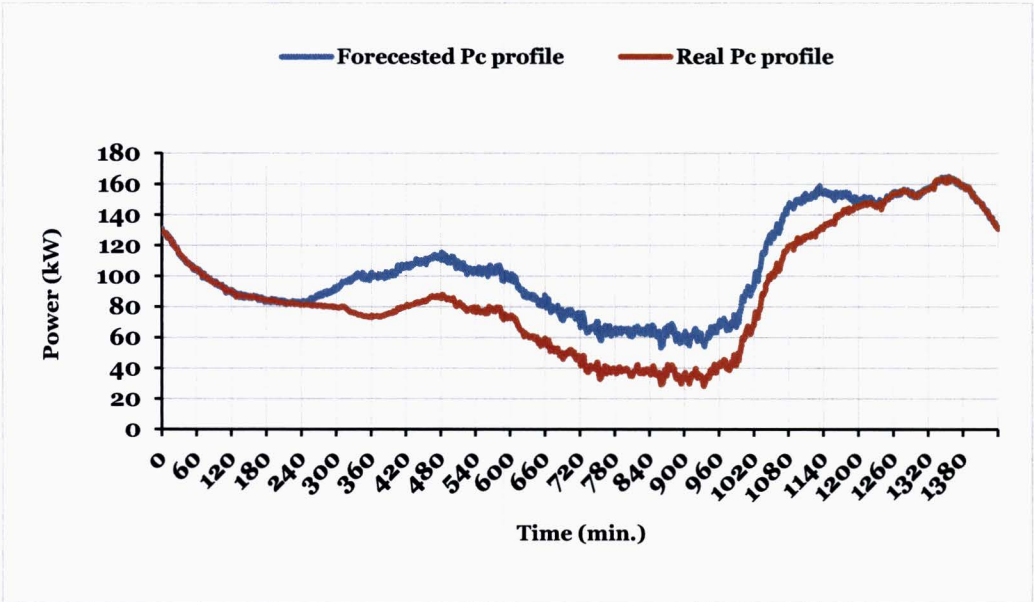

Figure 4.3 Pc summer profiles for small prediction error (RMSE=20) at the PV generation.

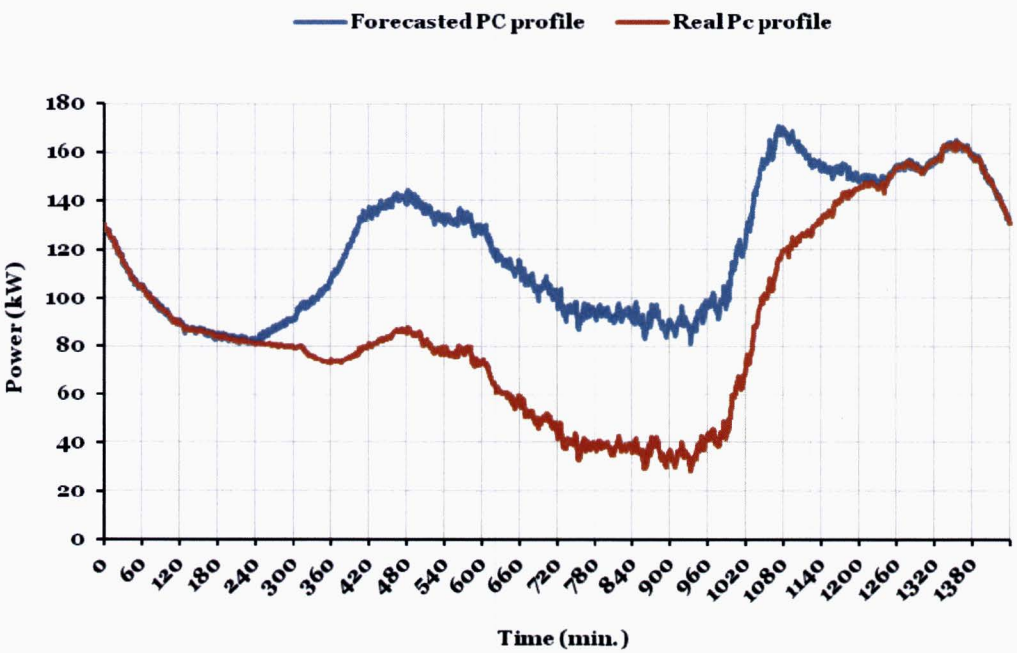

Figure 4.4 Pc summer profiles for large prediction error (RMSE=40) at the PV generation.

The second case study, is assumed to happen in the winter and examines the case where the household consumption is larger than forecasted and therefore the P_c measured is larger than expected ($dP_c > 0$).

This case is performed at the 12th January and the PV forecasted power profile and real profile are presented in Fig.4.5 and Fig. 4.6 for both small and large prediction errors.

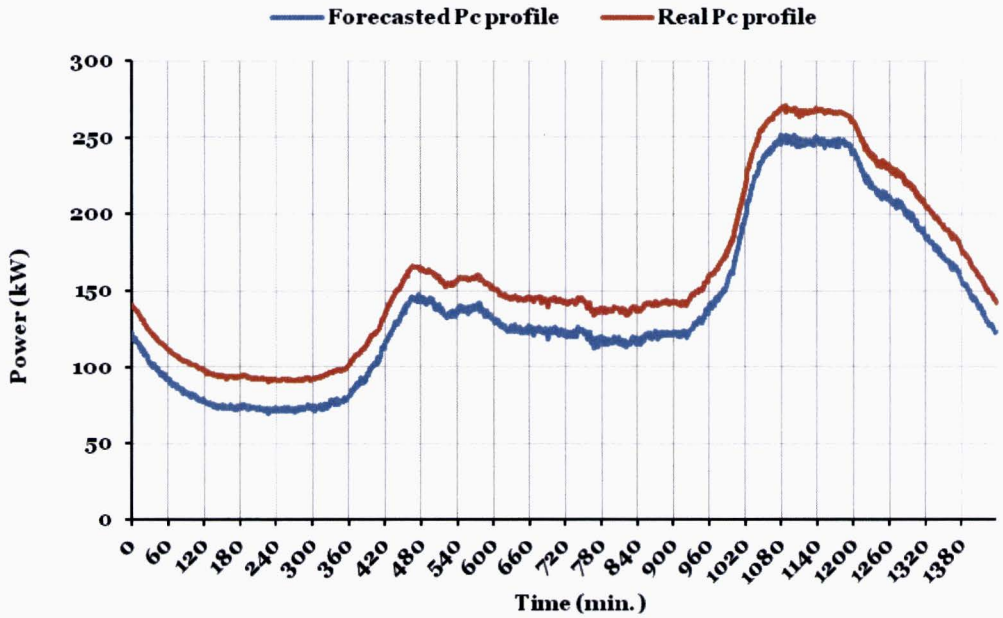

Figure 4.5 Pc winter profiles for small prediction error (RMSE=20) at the residential customers' consumption.

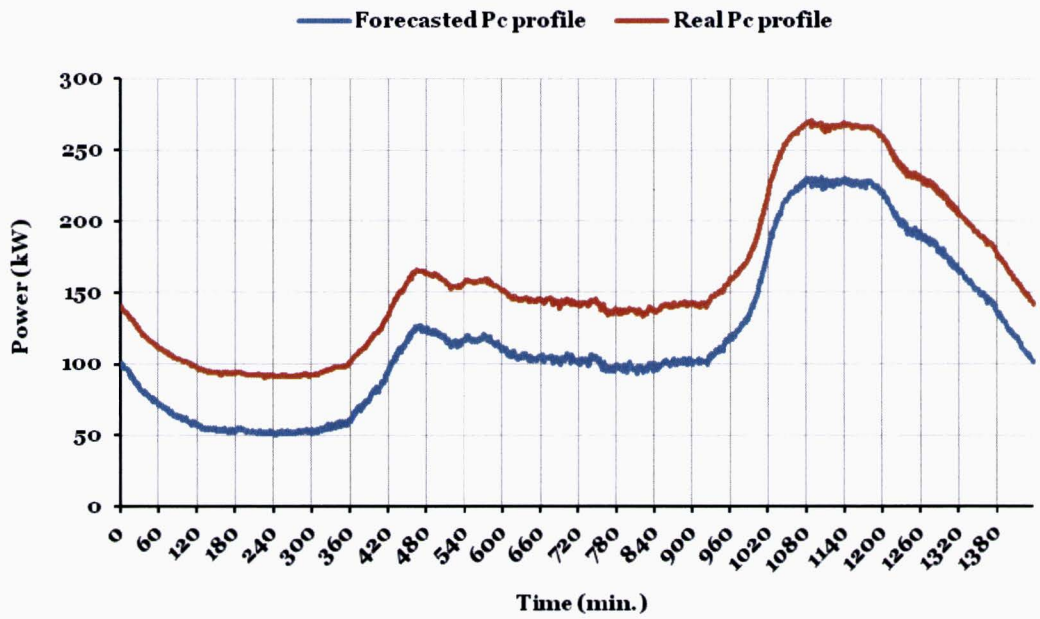

Figure 4.6 Pc winter profiles for large prediction error (RMSE=40) at the residential customers' consumption.

An overview of the case studies that are studied both for the summer and winter months are concentrated and presented in Table 4.2.

Table 4.2 Case studies for the intra-hour optimisation.

	State of the system	Pc profile
Case 1	Perfect prediction	Perfect prediction
Case 2	Erroneous prediction for the 1st PTU	Perfect prediction
Case 3a	Erroneous prediction for the 1st PTU	Erroneous prediction with small prediction error (RMSE =20)
Case 3b	Erroneous prediction for the 1st PTU	Erroneous prediction with large prediction error (RMSE =40)

As it is already mentioned, the only difference between the summer and the winter case studies is the dP_c, which is negative at the first occasion and positive at the second.

It can be seen at Table 4.2 that the prediction errors which are assumed for the state of the system consider only the 1st PTU. This assumption could be easily expanded to include errors for the state of even more PTUs, at the beginning of the horizon or even for all 48 PTUs. However, this would increase tremendously the complexity of the results. The scope of these case studies though is to give a better insight in the intra-hour algorithm and present its output when it receives wrong predictions. Therefore, it is believed that adding such complexity to the assumptions, even though it may lead to more realistic representations, is not desirable and would make the results confusing rather than explanative.

The case studies that were described in the table above are more thoroughly examined in the next sections.

4.4.1. Case Studies for the summer months

For the case studies that refer to the summer months, a date was selected randomly to equip the algorithms with realistic data from the Dutch TSO. Specifically, the case studies are performed based on data from the 30th of June 2012, and the optimisation starts at the 36th PTU of that date, i.e. at 9:00 a.m.

For the 1st case, the predictions are considered to be perfect, both for the state of the system and for the power profile at network point (c), the optimisation reacts as it is shown in Fig.4.7.

At the 1st PTU of the horizon (the 36th PTU of the day under examination), the imbalance price is very high and as the system state is 1 (request for upwards regulation), the BESS is being discharged with the maximum allowed power rate to maximise the revenues.

The next high imbalance price during the day is that referring to the 69th PTU, when the system also requires upwards regulation (state 1) and the BESS needs to react to that again by being fully discharged. In order to have the ability to be fully discharged at that PTU (with the maximum allowed power rate of 400kW) it needs to be charged at the previous PTUs to reach the maximum allowed *SoE* (i.e., *SoE*=0.9). As it can be seen in Fig. 4.7, even though the system states at the previous PTUs are 1 and 2 and pose a penalty for charging, the algorithm chooses the PTUs with the lowest penalising price, being the 37th, 44th, 47th, 48th and 51st respectively. In Fig. 4.8. it can be seen that the profits are the largest at the 69th PTU, while the losses due to the penalties for charging are much less.

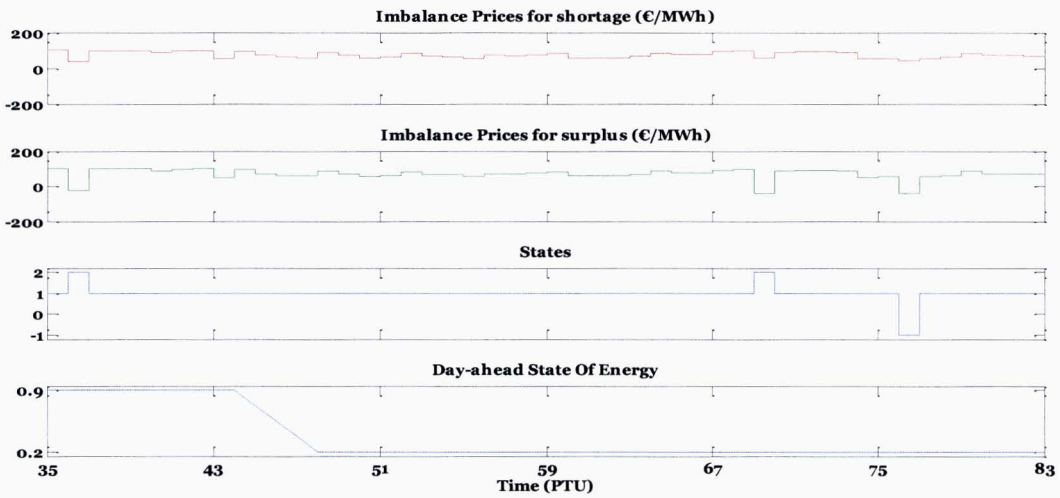

Figure 4.7 Input parameters for the 1st summer case study of the intra-hour optimisation problem.

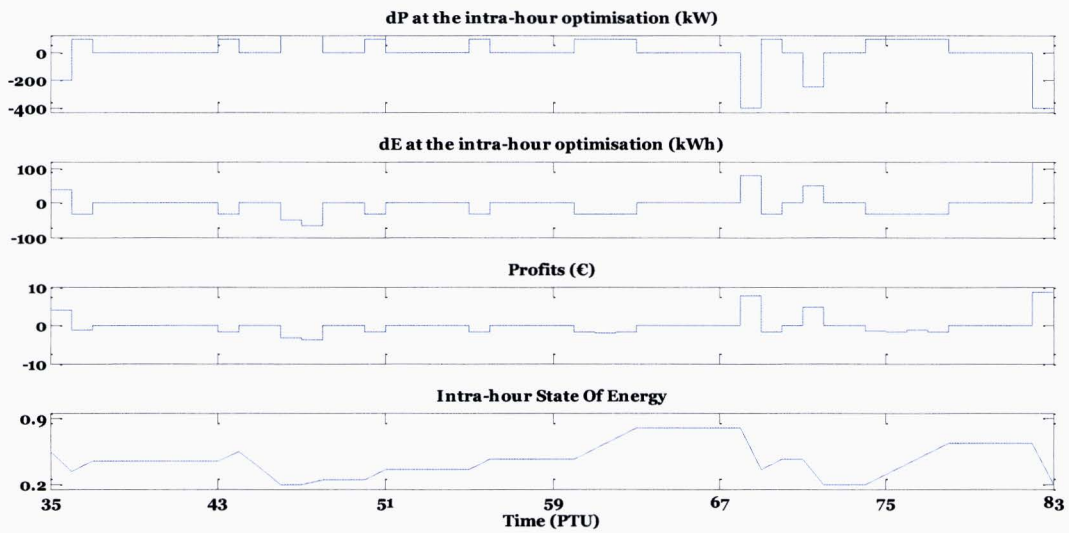

Figure 4.8 Outputs for the 1st summer case study of the intra-hour optimisation problem.

For the 2nd case, the prediction for the state of the system referring to the 1st PTU of the optimisation horizon (being the 36th of the day that is examined) is assumed to be erroneous, and the predicted state is considered 0. The basic difference that can be observed comparing with the results of the 1st case is that at the 1st PTU the algorithm decides not to schedule a discharging cycle as the state is now assumed to be 0, and any energy imbalance is going to be penalised. The discharging that was taking place during the 36th PTU in case 1, now takes place during the 39th and the 43rd PTUs. This is happening because at these PTUs the price is equal to the one in the 36th PTU, when the BESS was being discharged in case 1. For all the subsequent PTUs, within the optimisation horizon, the result of the BESS optimisation are identical with the previous case.

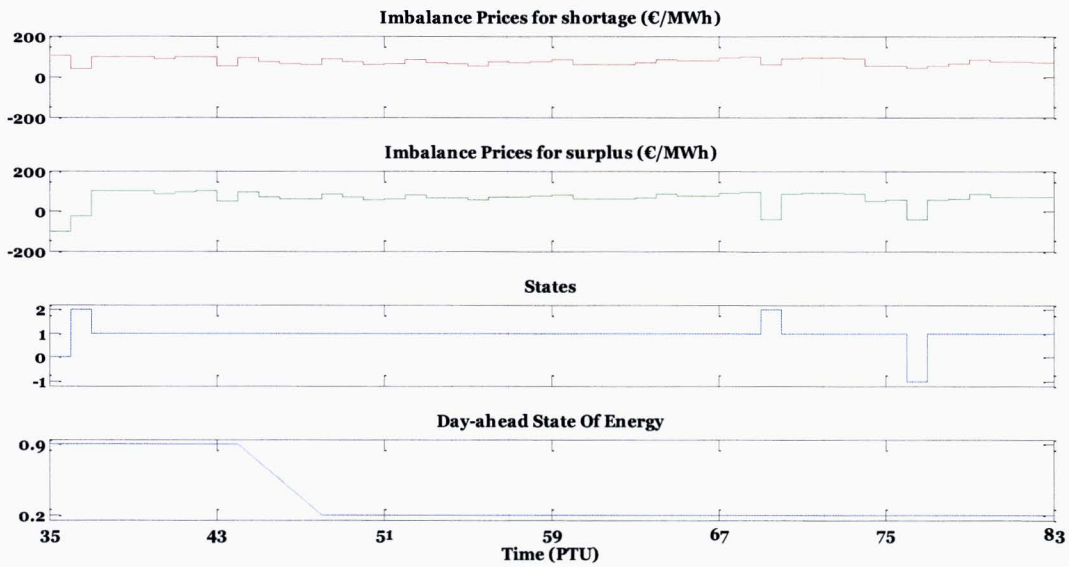

Figure 4.9 Input parameters for the 2nd summer case of the intra-hour optimisation problem.

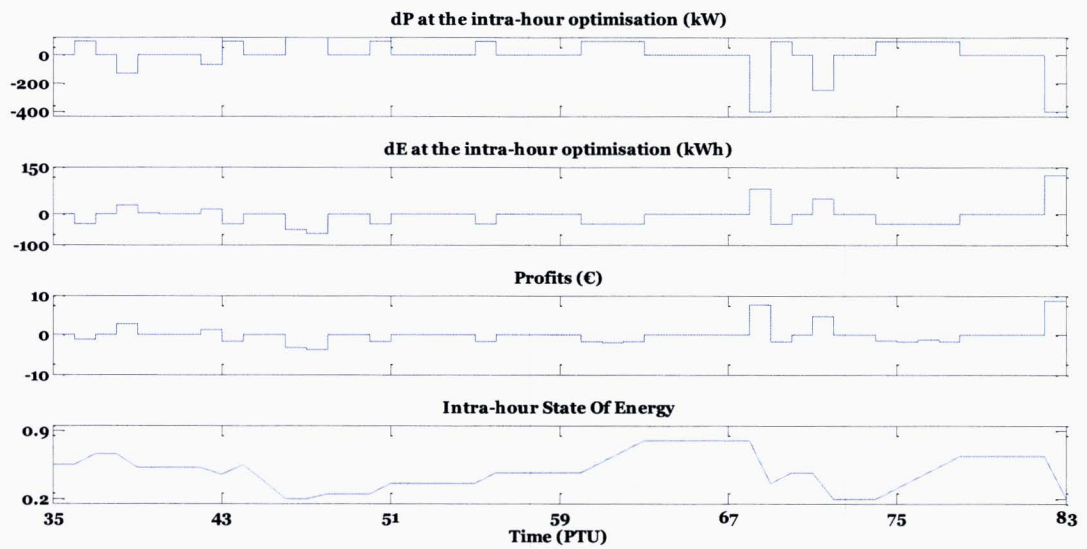

Figure 4.10 Outputs for the 2nd summer case of the intra-hour optimisation.

For the third case, an additional assumption is considered, that is that the prediction of the P_c power profile is erroneous as the PV generation is more than expected. Therefore, the power at network point (c) is less than its predicted value from the day-ahead schedule, resulting into an expected power imbalance $dP_c < 0$. As the state of the system is predicted to be 0, during the first PTU, the energy imbalance should be kept 0 to avoid penalising costs, and therefore the battery is scheduled to be charged in order to create an imbalance ($dP_b > 0$) equal and opposite to dP_c, as $dE = -(dP_c + dP_b) \cdot \tau_s$. This can be seen in Fig. 4.12 and Fig. 4.14 for both large and small errors in the prediction of the PV generation.

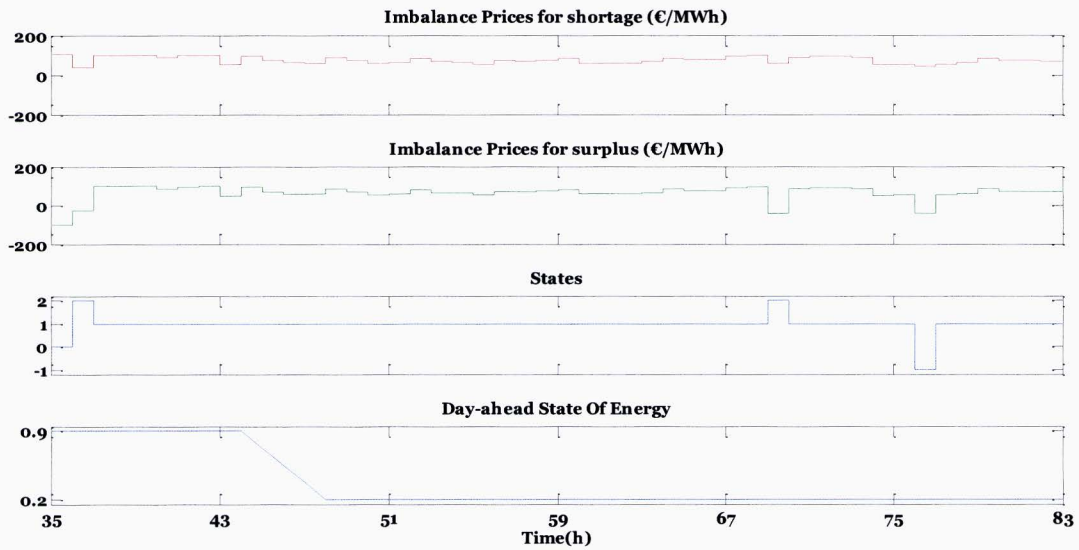

Figure 4.11 Input parameters for the 3rd summer case of the intra-hour optimisation problem for small prediction error.

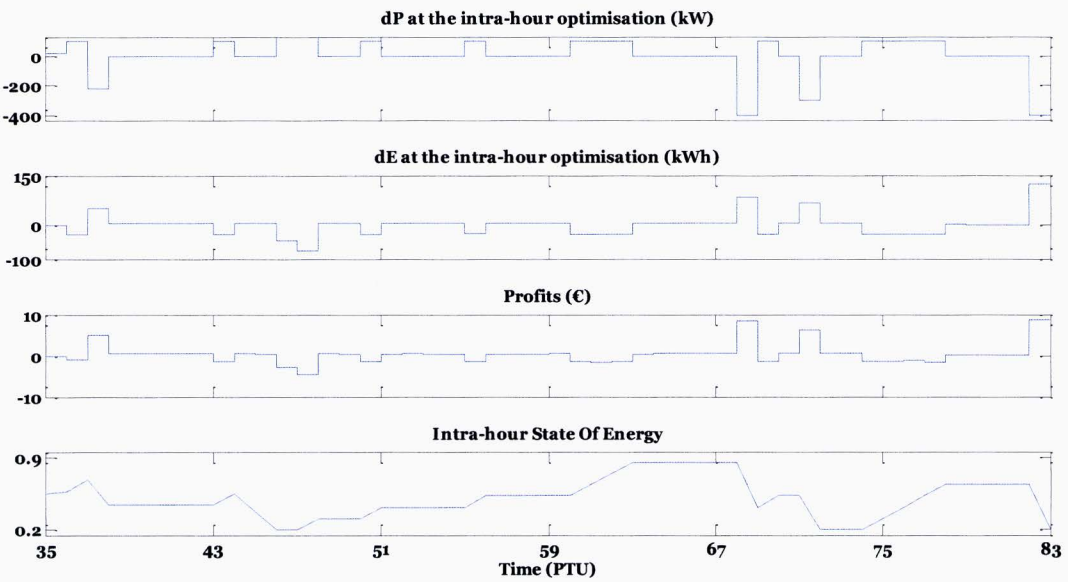

Figure 4.12 Output of the 3rd summer case of the intra-hour optimisation for small prediction error.

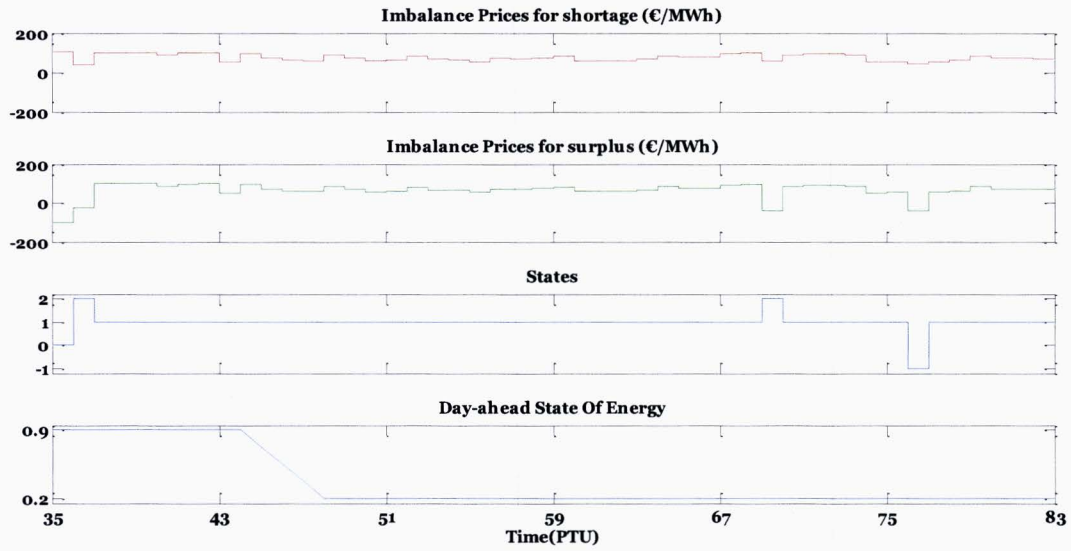

Figure 4.13 Input parameters for the 3rd summer case of the intra-hour optimisation problem for large prediction error .

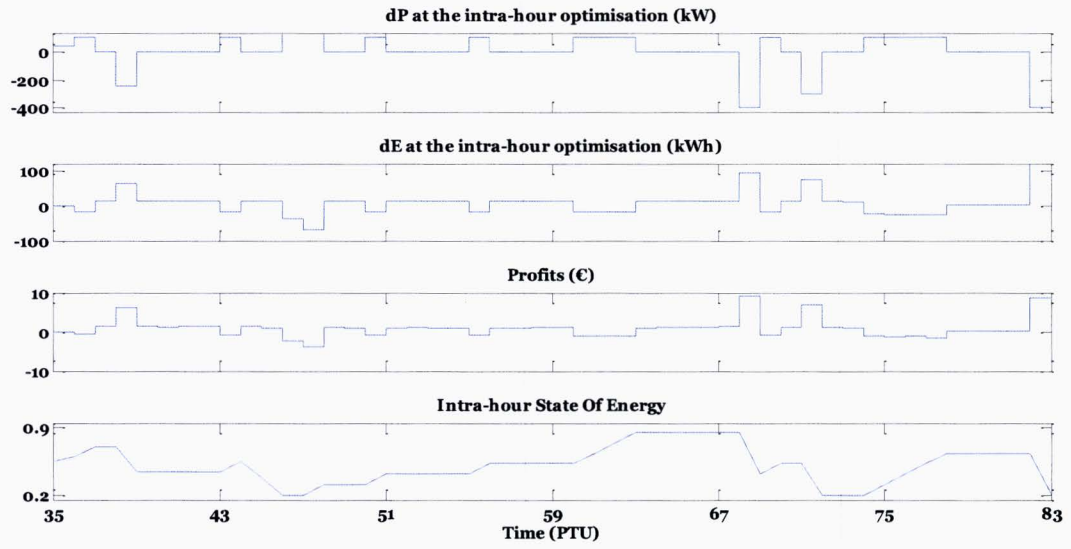

Figure 4.14 Output of the 3rd summer case of the intra-hour optimisation for large prediction error.

4.4.2. Case Studies for the winter months

For the first winter case study, there are no prediction errors assumed. At the 1st PTU of the horizon, the system requires upwards regulation (state=1) and the BESS is scheduled to be fully discharged. The next price that the aggregator wants to take advantage of, is the one during the 3rd PTU, within the optimisation horizon, when the BESS should be discharged again. As this would not be possible if its *SoE* remains at the lowest limit, i.e., *SoE*=0.2, therefore the algorithm decides to schedule a charging cycle during the 2nd PTU of the optimisation horizon, Even though the state is expected to be 2 and any imbalance will be penalised, the penalising price for charging at that time is rather low compared with the rewarding price of the subsequent PTU. The same pattern is being followed by the optimisation algorithm for the rest PTUs of the horizon. Fig. 4.15 and 4.16 show the inputs and the outputs of the intra-hour optimisation for the 1st winter case study.

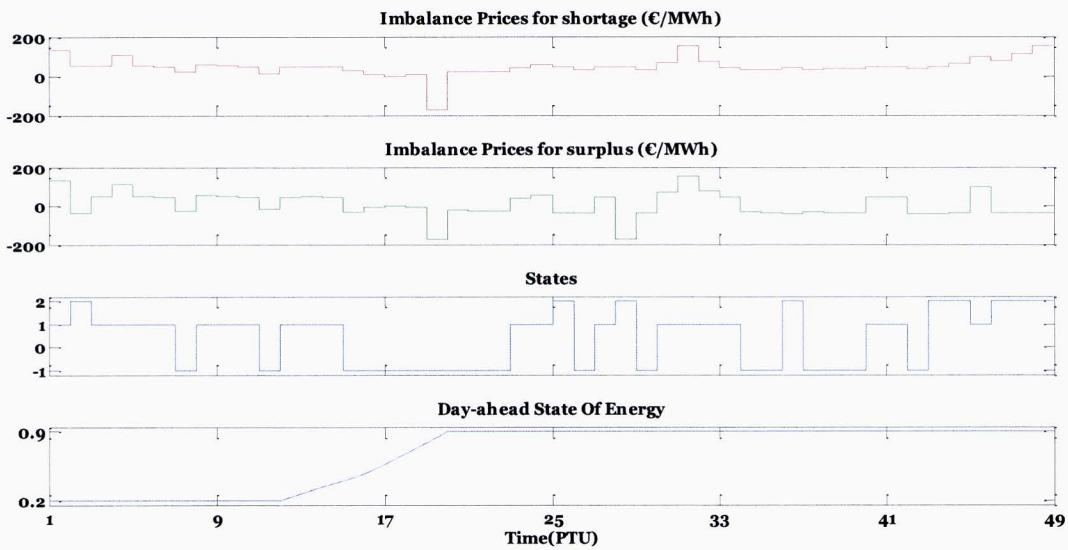

Figure 4.15 Input parameters for the 1st winter case study of the intra-hour optimisation problem.

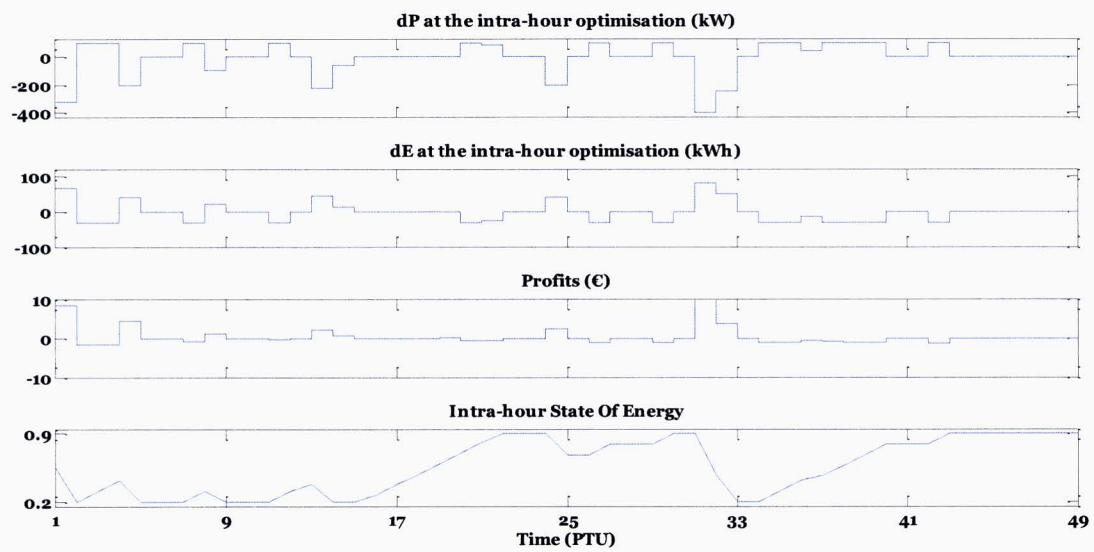

Figure 4.16 Output of the 1st winter case study of the intra-hour optimisation.

Figures 4.17 and 4.18 show the input and output of the 2nd case study. Having the same assumption as in the 2nd case of section 4.4.1. a wrong prediction is considered for the 1st PTU's state of the system, which is forecasted to be 0. As every energy imbalance is penalised when the state is 0, the BESS is not being discharged, as it was in the previous case study, and the dP_b remains 0. For the remaining PTUs of the optimisation horizon, the BESS follows the same profile as in case 1.

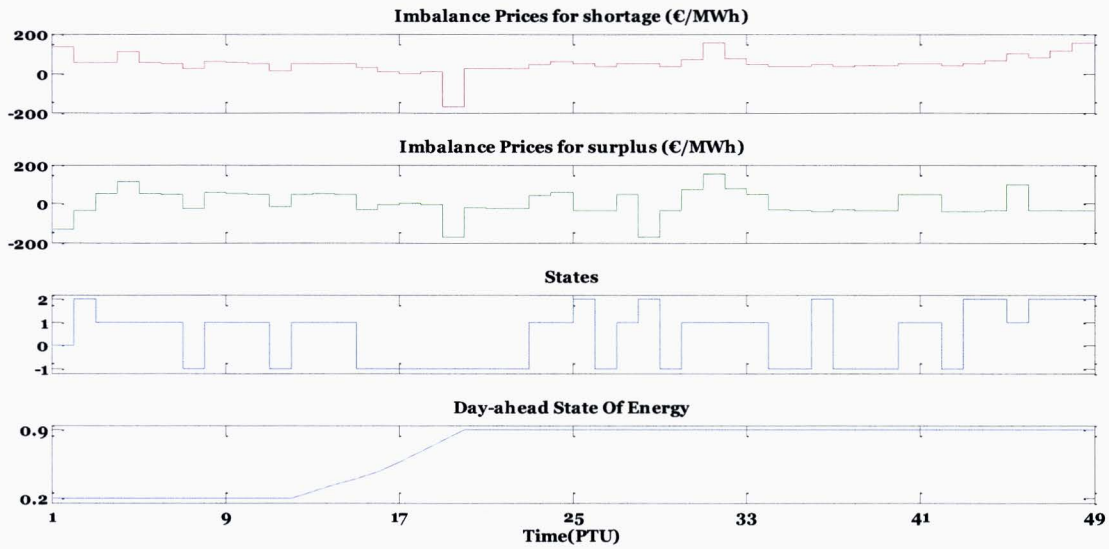

Figure 4.17 Input parameters for the 2nd winter case study of the intra-hour optimisation problem.

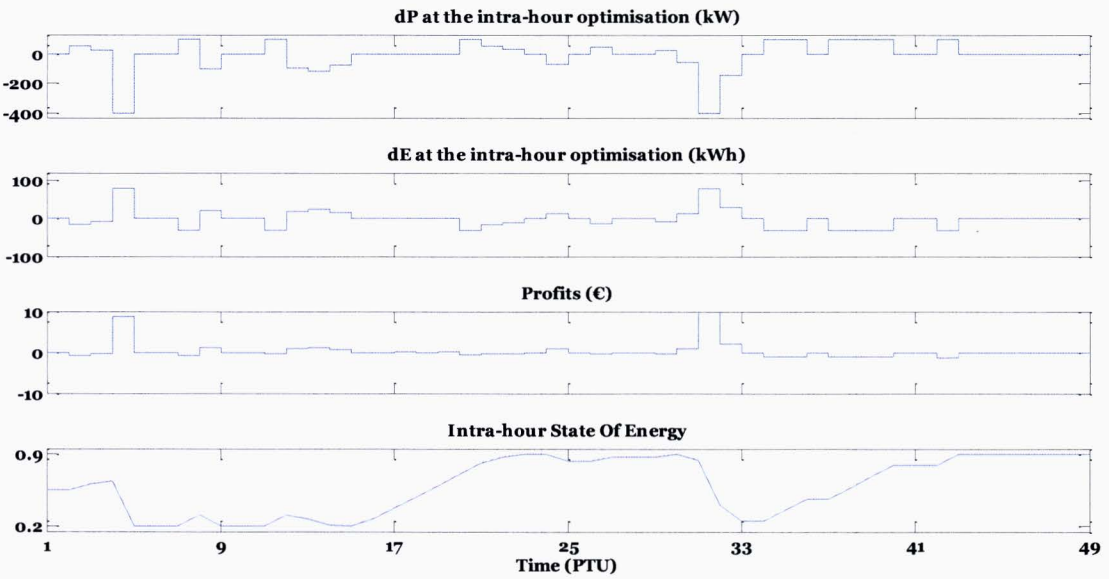

Figure 4.18 Output of the 2nd winter case study of the intra-hour optimisation.

For the 3rd case, an erroneous prediction for the P_c power profile is also included. At that time, the residential customers' power profile is expected to exceed the predicted values. This leads to a positive imbalance with respect to the power profile at network point (c) ($dP_c > 0$). As the state of the system is still assumed to be 0, this energy imbalance has to be cancelled out by the BESS in order to keep the overall energy imbalance dE to 0. In order to achieve this, the BESS is being discharged with a rate that results the dP_b to be equal and opposite to the dP_c. The figures 4.19-4.22 present the BESS behaviour for large and small prediction errors.

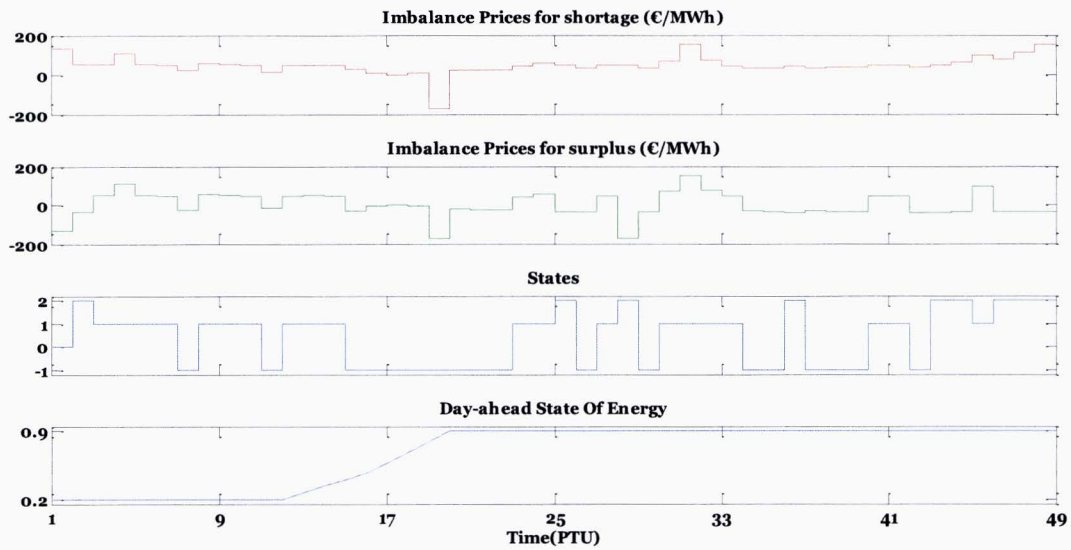

Figure 4.19 Input parameters for the 3rd winter case study of the intra-hour optimisation problem for small prediction error.

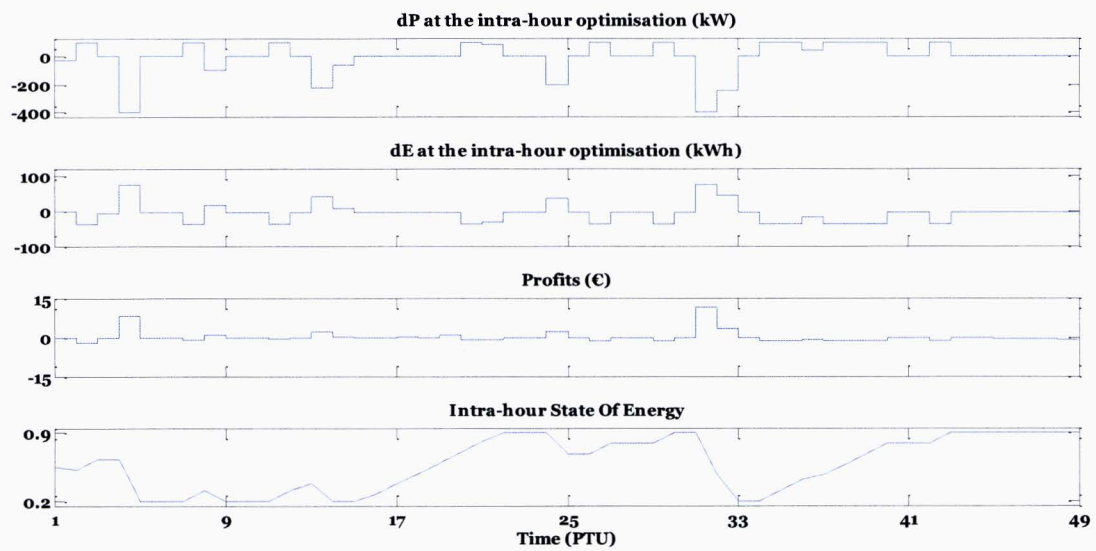

Figure 4.20 Output of the 3rd winter case study of the intra-hour optimisation for small prediction error.

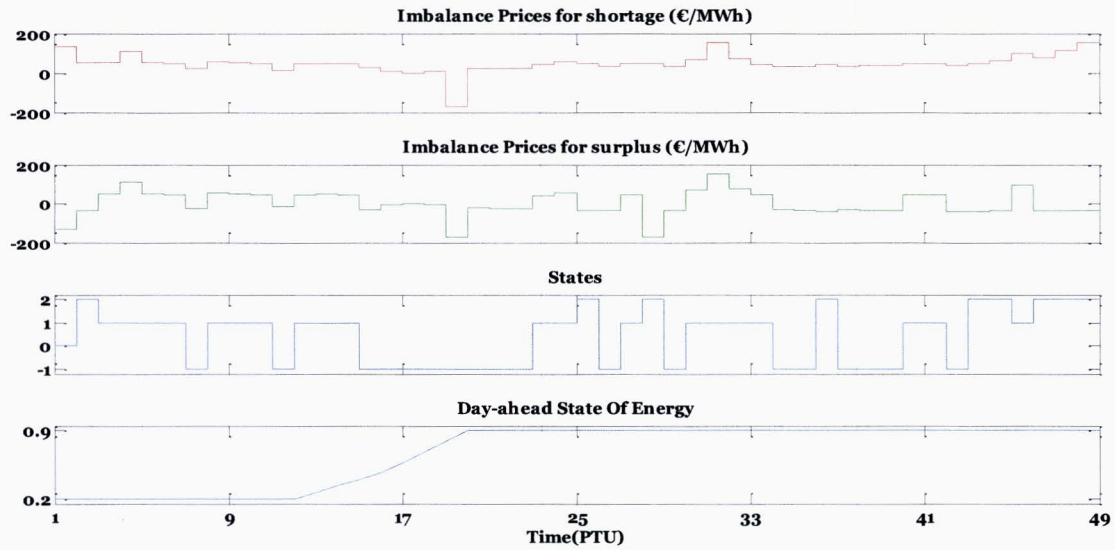

Figure 4.21 Input parameters for the 3rd winter case study of the intra-hour optimisation problem for large prediction error.

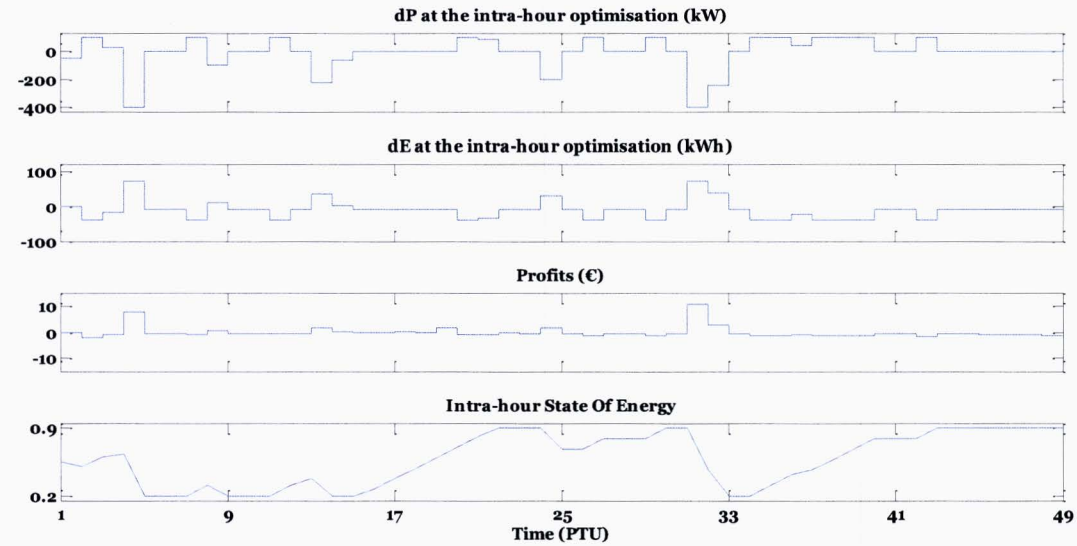

Figure 4.22 Output of the 3rd winter case study of the intra-hour optimisation for large prediction error.

The case studies presented in 4.4.1 and 4.4.2. illustrate that the algorithm is able to adapt to the scheduling of the charging and discharging cycles under updated forecasts and maximise the revenues or minimise the losses for the optimisation horizon. This is particularly useful particularly for real life simulations, as it takes into consideration updated forecasts of residents' behavior and generation from stochastic processes (i.e., PV generation) and acts accordingly.

4.5. Economic impact of imbalances

Table 4.3 captures the daily profits and losses for a randomly selected day from the year 2012, i.e., the 26th of June. At that day, a deviation is assumed to appear for the power profile at network point (c) between the predicted and the measured value, causing a power imbalance dP_c. This example examines the economic impact that a positive or negative power imbalance can have on the investigated system. The absolute value of dP_c is considered to be equal to the value that was defined in section 4.3 with respect to large prediction error (RMSE=40).

As it can be seen in table 4.3, when there is no power imbalance at network point (c), the daily profit is 37.95€. A negative imbalance though, raises the daily profit to 40.44€ while a positive one leads to decreased profits of 20.52€.

The reason for this is that at the 26th June, the state of the system was 1 for most PTUs of the day which means that most of the time the aggregator had an incentive to maintain a positive imbalance ($dE > 0$) to benefit from passive contribution. In the case that the dP_c is negative, the energy imbalance that occurs is positive as $dE = -(dP_c + dP_b) \cdot \tau_s$ and leads to increased profits, whereas in the case that the imbalance is positive the energy imbalance is negative and leads to reduced profits or even financial losses. Therefore, it is expected that in such a day, a negative dP_c is more beneficial than a negative one as it contributes to the overall system balance.

Table 4.3 Profits and losses that occur at a random day (26th June) from the participation of the system in the Tennet balancing market.

Imbalance	Daily profits/losses including the BESS(€)	Daily profits/losses without the BESS(€)
dPc=0	37.95	0
dPc>0	20.52	-24.78
dPc<0	40.44	-14.38

The results presented in Table 4.3 illustrate the importance of the BESS combined with renewable energy sources in terms of financial impact for the aggregator. Considering the case where the aggregator represents only the residential customers and the PV generators (excluding the BESS), any power imbalance that would occur at network point (c) would lead to penalties or rewards in a stochastic way to which the aggregator would not be able to react. The presence of the BESS though adds flexibility to the system, and the algorithms decide whether to utilise that flexibility to cancel out any expected imbalance that is considered to be undesired, or to contribute even more to increase the total imbalance dE when it is expected to bring additional revenues through passive contribution. The importance of the BESS presence is also depicted in the results of the above-mentioned example where it can be seen that regardless of the energy imbalance, the contribution of the BESS is significant in terms of improved financial performance.

4.6. Economic assessment of the intra-hour optimisation

In multi-level optimisation (i.e. day-ahead schedule in advance), part of the capacity of the battery might be committed for certain hours. In some cases these commitments *a priori* might lead to larger energy imbalances during the intra-hour optimisation that can be beneficial for the system balance, and result in additional revenues. In other occasions though, it might limit the options for the BESS to respond close to real-time and therefore might bound the potential profits. Since the answer to such a question cannot be answered in a deterministic way due to the stochastic nature of energy processes and power system procedures (what the state of the system might be at each time period that the battery is committed to be charged or discharged), it is not easy to decide which is the optimal approach.

In order to create an insight into this topic, an analysis is run for several years in order to compare the estimated annual revenues between two potential applications: the case of an hierarchical multilevel optimisation approach, where the intra-hour optimisation is performed after the day ahead optimisation, and the case of a stand-alone intra-hour optimisation approach.

Table 4.4 Annual revenues for the approach of stand-alone intra-hour optimisation and hierarchical multilevel optimisation.

Year	Annual Revenues (€) (with day-ahead on top)	Annual Revenues (€) (without day-ahead on top)
2012	23748	27443
2011	18817	21725
2010	12434	14750
2006	24816	30424
2003	20164	25259

Table 4.4 depicts the calculated annual revenues for each distinct case. It can be seen that, for every year that was examined, the revenues at the case of a stand-alone intra-hour optimisation are more than those in the case of an hierarchical multi-level approach. This indicates that if the capacity which has been committed due to the day-ahead optimisation could be fully exploited during the intra-hour optimisation then it would leads to more profits. Therefore it seems that from a financial point of view, a single intra-hour schedule is the most preferable solution.

This assessment is valid though in the case of rather accurate predictions for the intra-hour state of the system and the imbalance prices. However, due to the stochastic nature of the imbalance market, these predictions are inherently very difficult to be assumed perfect. On the other hand, the task of creating rather accurate predictions of the day-ahead price dynamics is more plausible as the day-ahead market follows a more regular pattern.

Chapter 5 Real-time operations

5.1. Real-time Planning

As mentioned in the previous section, in real-time operations the aggregator has to comply with the *a priori* defined power schedule $P_a^{das}(l)$, l=1,..., 96, for each settlement period (τ_s = 15 min.) of the operational day, whereas any mismatch from the submitted schedule will be regarded as an energy imbalance $\Delta E(l)$ for the l^{th} settlement period.

$$P_a^{das}(l)\cdot\tau_s - \sum_{t=i_l}^{i_{l+1}-1} P_a^{msr}(t)\cdot\tau = \Delta P_a(l)\cdot\tau_s = \Delta E(l) \qquad (5.1)$$

where $P_a^{msr}(t)$ is the actual measured power at network point (a) and at control period t, i_l=15·(l−1)+1 corresponds to the first control period of the l^{th} settlement period, and $t \in [i_l, i_{l+1}-1]$.

In real-time, the aggregator is tracking any deviations from the submitted *day-ahead* schedule $P_a^{das}(l)$ by using (5.2). Considering that the current time instant is k, during the l^{th} settlement period of the day, the aggregator obtains the actual measurements at network points (a) and (b), and calculates the power at network point (c) by using (1.1)(2.1). Then, the forecast of the power trajectory $P_c^{rts}(k+i\,|\,k)$ is acquired for the control horizon i=1, ..., $i_{horizon}$. Any expected energy imbalance $\Delta E(l)$ at the end of the l^{th} settlement period can be expressed through an energy balance equation:

$$P_a^{das}(l)\cdot\tau_s - \sum_{t=15\cdot(l-1)+1}^{k} P_a^{msr}(t)\cdot\tau - \sum_{i=1}^{15\cdot l-k} P_a^{rts}(k+i\,|\,k)\cdot\tau = \Delta E(l) \qquad (5.2)$$

where the first term in (5.2) represents the energy volume which has been cleared in the *day-ahead* market for the l^{th} settlement period, the second term represents the accumulated energy content up to current time instant k (based on actual measurements since the beginning of the l^{th} settlement period), and the third term represents the expected accumulated energy from current time instant k until the end of the l^{th} settlement period.

In theory, the aggregator's goal is to cancel any energy imbalance $\Delta E(l)$ by the end of the l^{th} settlement period. However, as mentioned in the previous section, when the system state is explicitly *short* or *long* during the l^{th} settlement period, then the aggregator might try to minimise or maximise the energy imbalance $\Delta E(l)$ to benefit from passive contribution. To achieve this, in real-time, the aggregator coordinates the BESS operation by determining a set-point power trajectory that the power output should ideally follow from current time instant k and until the end of the l^{th} settlement period. This set-point power trajectory $P_b(k+i|k)$, for i=1, ..., 15·l−k can be calculated by using (5.3):

$$P_a^{das}(l)\cdot\tau_s - \sum_{t=15\cdot(l-1)+1}^{k} P_a^{msr}(t)\cdot\tau - \sum_{i=1}^{15\cdot l-k} (P_c^{rts}(k+i\,|\,k) + P_b^{rts}(k+i\,|\,k))\cdot\tau = \Delta E(l) \qquad (5.3)$$

The set-point trajectory $P_b(k+i|k)$ can be written as:

$$P_b^{rts}(k+i|k) = P_b^{das}(k+i) + dP_b^{rts}(k+i|k) \qquad (5.4)$$

where $P_b^{das}(k+i)$ reflects the power set-points defined during the day-ahead optimisation, i.e. $P_d^{das}(h)$, whereas $dP_b^{rts}(k+i|k)$ is a deviation set-point which is defined in real-time. The optimisation objective of the *real-time* problem is to maximise the objective function:

$$\max_{dP_d^{ihs}(k+i|k)} J \qquad (5.5)$$

The profit function J is defined in (5.6):

$$J = \Delta E(l) \cdot \pi_{imb}^{prd}(l) + (SoE_{mpc}^{rts}(15 \cdot l + 1) - SoE_{ref}^{rts}(15 \cdot l + 1)) \cdot E_{nom} \cdot \pi_{imb}^{prd}(l+1) \qquad (5.6)$$

where the first term in (5.6) reflects the expected profits to be obtained through the imbalance settlement system for the l^{th} settlement period, whereas the last term is meant to penalise any deviations from the expected *intra-hour* optimised *SoE* at the end of the control horizon. The control horizon in the real time problem is set to be 15 time units of 1 minute, contrary to the real time problem. Note that, in *real-time*, the predicted state of the system $s^{prd}(l)$ might change which will subsequently influence the imbalance price $\pi_{imb}^{prd}(l)$ that the aggregator will face.

The resulted quarterly charging states of the *intra-hour* optimisation problem $SoE_{ref}^{ihs}(l)$, for l=1,..., 96, are transformed on a per minute basis by using (5.7):

$$SoE_{ref}^{rts}(t) = SoE_{ref}^{ihs}(l) + \frac{SoE_{ref}^{ihs}(l+1) - SoE_{ref}^{ihs}(l)}{15} \cdot (i - 1 - 15 \cdot (l-1)) \qquad (5.7)$$

where $t \in [i_l, i_{l+1} - 1]$ for each lth settlement period, l=1, ..., 96.

As mentioned before, the second term of the objective function is meant to give an economic value to the deviation of the *SoE* at the end of the l^{th} PTU from its expected $SoE_{ref}^{ihs}(l)$. In order to accomplish that, the imbalance price $\pi_{imb}^{prd}(l+1)$ has to be defined accordingly so that this term acts as a rewarding or a penalising term, depending on the occasion. For example, if the state of the $(l+1)^{th}$ PTU is predicted to be 1 (upwards regulation), a positive deviation of the *SoE* ($dSOE_{rts}(l) > 0$) would mean that more capacity of the BESS is available for discharging, and therefore it should be rewarded. On the other hand, if the deviation of the *SoE* is negative ($dSOE_{rts}(l) < 0$) it should be penalised.

The definition of these imbalance prices for the real-time optimisation problem is provided in Table 5.1.

Table 5.1 Real time optimisation pseudo code: imbalance prices definition.

```
1.  begin;
2.  # Current settlement period is q (e.g., the last settlement period of the operational planning day), whereas τs =
    15 min., m= 1, ..., 48.
3.  # dSOE_rts(l) is the deviation from the expected intra hour optimised SOE at the end of the control horizon.
4.    if s^prd(l+1) = 0 then
5.      if dSOE_rts(l) > 0 then
```

6. $\pi_{imb}^{prd}(l+1) = \pi_{surpl}^{prd}(l+1) = -\text{abs}(\pi_{mid}^{prd}(l+1) - \pi_{ic}^{prd}(l+1))$ **else**

7. **if** $dSOE_{rts}(l) < 0$ **then**

8. $\pi_{imb}^{prd}(l+1) = \pi_{short}^{prd}(l+1) = \text{abs}(\pi_{mid}^{prd}(l+1) + \pi_{ic}^{prd}(l+1))$

9. **end if**

10. **if** $s^{prd}(l+1) = 2$ **then**

11. **if** $dSOE_{rts}(l) > 0$ **then**

12. $\pi_{imb}^{prd}(l+1) = \pi_{surpl}^{prd}(l+1) = -\text{abs}(\pi_{-}^{prd}(l+1) - \pi_{ic}^{prd}(l+1))$ **else**

13. **if** $dSOE_{rts}(l) < 0$ **then**

14. **if** (emergency power is called) **then**

15. $\pi_{imb}^{prd}(l+1) = \pi_{short}^{prd}(l+1) = \text{abs}(\max(\pi_{+}^{prd}(l+1), \pi_{em}^{prd}(l+1)) + \pi_{ic}^{prd}(l+1))$

16. **else** $\pi_{imb}^{prd}(l+1) = \pi_{short}^{prd}(l+1) = \text{abs}(\pi_{+}^{prd}(l+1) + \pi_{ic}^{prd}(l+1))$

17. **end if**

18. **end if**

19. **if** $s^{prd}(l+1) = -1$ **then**

20. **if** $dSOE_{rts}(l) > 0$ **then**

21. $\pi_{imb}^{prd}(l+1) = \pi_{surpl}^{prd}(l+1) = -abs(\pi_{-}^{prd}(l+1) - \pi_{ic}^{prd}(l+1))$ **else**

22. **if** $dSOE_{rts}(l) < 0$ **then**

23. $\pi_{imb}^{prd}(l+1) = \pi_{short}^{prd}(l+1) = \pi_{-}^{prd}(l+1) + \pi_{ic}^{prd}(l+1)$ **else**

24. **end if**

25. **if** $s^{prd}(l+1) = +1$ **then**

26. **if** $dSOE_{rts}(l) > 0$ **then**

27. **if** (emergency power is called) **then**

28. $\pi_{imb}^{prd}(l+1) = \pi_{surpl}^{prd}(l+1) = \max(\pi_{+}^{prd}(l+1), \pi_{em}^{prd}(l+1)) - \pi_{ic}^{prd}(l+1)$

29. **else** $\pi_{imb}^{prd}(l+1) = \pi_{surpl}^{prd}(l+1) = \pi_{+}^{prd}(l+1) - \pi_{ic}^{prd}(l+1)$

30. **end if**

31. **if** $dSOE_{rts}(l) < 0$ **then**

32. **if** (emergency power is called) **then**

33. $\pi_{imb}^{prd}(l+1) = \pi_{short}^{prd}(l+1) = \max(\pi_{+}^{prd}(l+1), \pi_{em}^{prd}(l+1)) + \pi_{ic}^{prd}(l+1)$

34. **else** $\pi_{imb}^{prd}(l+1) = \pi_{surpl}^{prd}(l+1) = \pi_{+}^{prd}(l+1) + \pi_{ic}^{prd}(l+1)$

35. **end if**

36. **end if**

37. **end for**

38. # The iteration continues with the next settlement period and the whole process is repeated.

39. $l = l+1$

40. **end**

The simulation of the real-time algorithm lasts on average a total time of 18 s. in the aforementioned software which means that it is fast enough to be implemented in control procedures with a control step of one minute as proposed in this investigation. Furthermore, within the hierarchical multi-level optimisation approach, the output of the *SoE* from the last real-time simulation at a certain PTU (i.e., the 15th minute of each PTU) is applied as an input to the intra-hour optimisation for the following PTUs.

5.2. Real time case studies

The cases that are going to be studied in this chapter are the same as the ones in Chapter 4. For both summer and winter months, erroneous predictions are assumed for the state of the system at the 1st PTU of the optimisation horizon and for the power profile at network point (c). In this chapter however, one more case study is examined, in which at a certain minute during the PTU (i.e. the 10th) the prediction of the system state is updated and the aggregator responds to that accordingly. Table 5.2 presents the case studies that are examined throughout the chapter.

Table 5.2 Overview of the case studies for the real-time optimisation problem.

	State of the system	**Pc profile**
Case 1	Erroneous prediction for the 1st PTU	Perfect prediction
Case 2a	Erroneous prediction for the 1st PTU	Erroneous prediction with small prediction error (RMSE =20)
Case 2b	Erroneous prediction for the 1st PTU	Erroneous prediction with large prediction error (RMSE =40)
Case 3a	Erroneous prediction for the 1st PTU, corrected at the 10th minute	Erroneous prediction with small prediction error (RMSE=20)
Case 3b	Erroneous prediction for the 1st PTU, corrected at the 10th minute	Erroneous prediction with large prediction error (RMSE=40)

These case studies are examined for both situations of winter and summer months. Their only difference is that during the winter case the aggregate residential customers' load is overestimated which results to power imbalances $dP_c > 0$, while the summer case considers overestimations of the PV generation which results to power imbalances $dP_c < 0$.

5.2.1. Real time case studies for the summer months

At the first case, an erroneous prediction for the system state is assumed for the 1st PTU, while the prediction of the power profile P_c is considered perfect. As the state of the system is 0 at the 1st PTU, the control system of the BESS is keeping the dP_b to 0, to avoid additional imbalances and subsequent financial penalties.

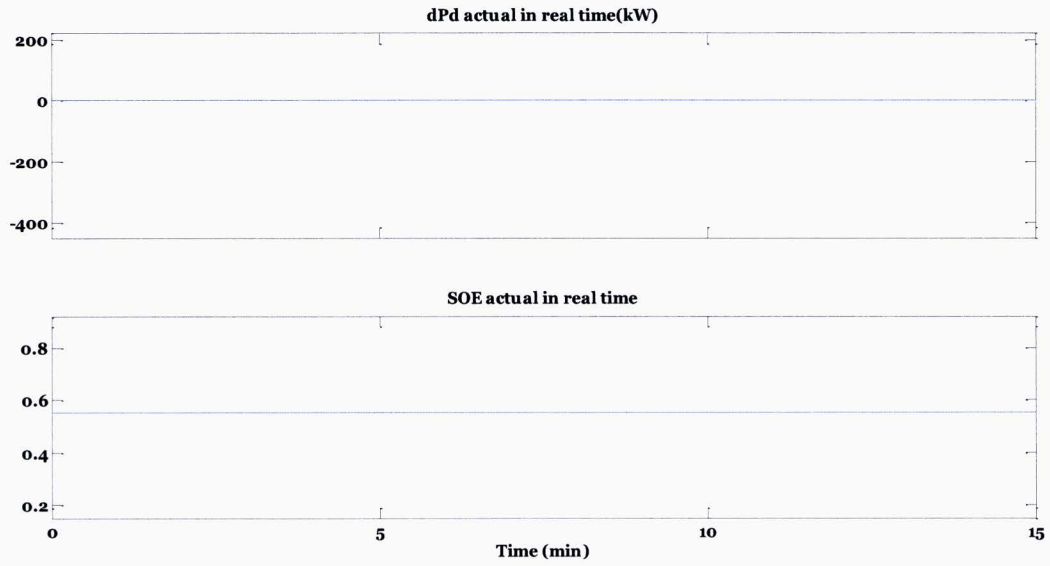

Figure 5.1 Power profile and SoE of the BESS for the 1st summer case study according to the real-time optimisation (30th June, 2012).

At the next case, the assumption of erroneous predictions for the PV generation and as a result in the P_c power profile is considered. As the state of the system is still wrongly predicted to be 0, the aggregator tries to minimise the energy imbalance dE and therefore the output of the algorithm, i.e., the power deviation value dP_b, is equal and opposite to the dP_c power value. The Fig. 5.2 and 5.3 show the result of the real-time optimisation for both small and large prediction errors (cases 2a and 2b in Table 5.2).

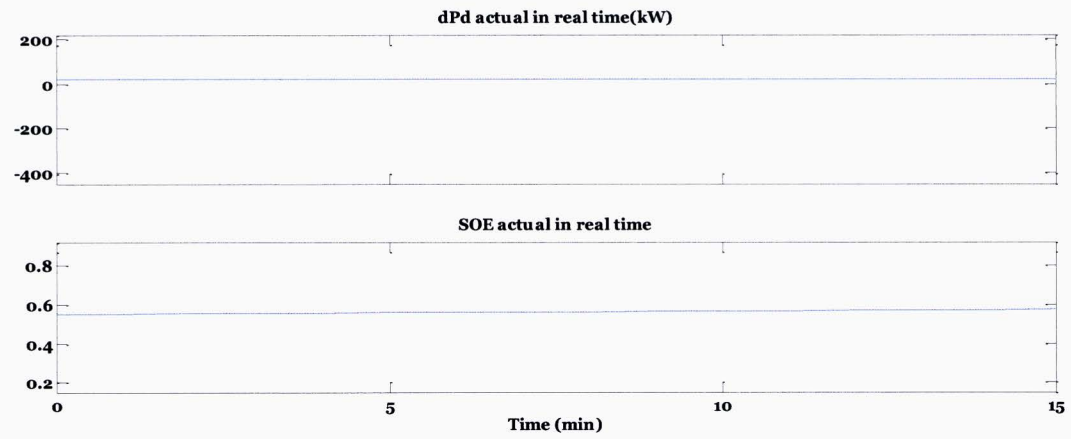

Figure 5.2 Power profile and SoE of the BESS for summer case 2a according to the real time optimisation (30th June, 2012).

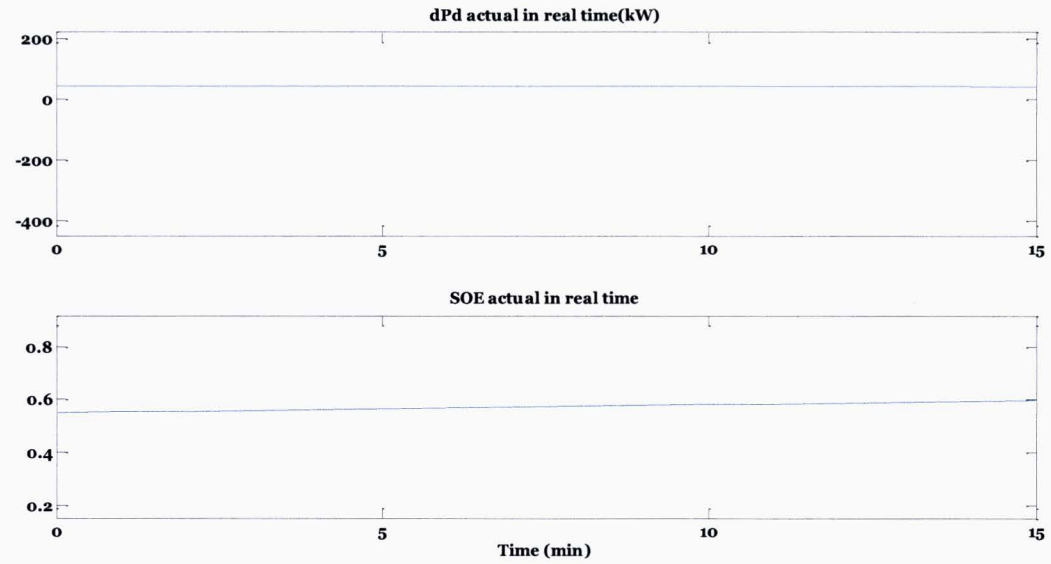

Figure 5.3 Power profile and SoE of the BESS for summer case 2b according to the real time optimisation (30th June, 2012).

The 3rd case examines how the algorithm reacts to the updated predictions that the aggregator receives during the PTU. Specifically, while at the first 10 minutes the prediction is wrong as in cases 1 and 2 and assumes the system state to be 0, at the 11th minute there is an updated prediction that defines the state of the system to be 1. This means that the system requires upwards regulation and the BESS reacts to that by being discharged. Fig. 5.4 and 5.5 depict this reaction for both small and large errors in the prediction of the power profile P_c (cases 3a and 3b in Table 5.2).

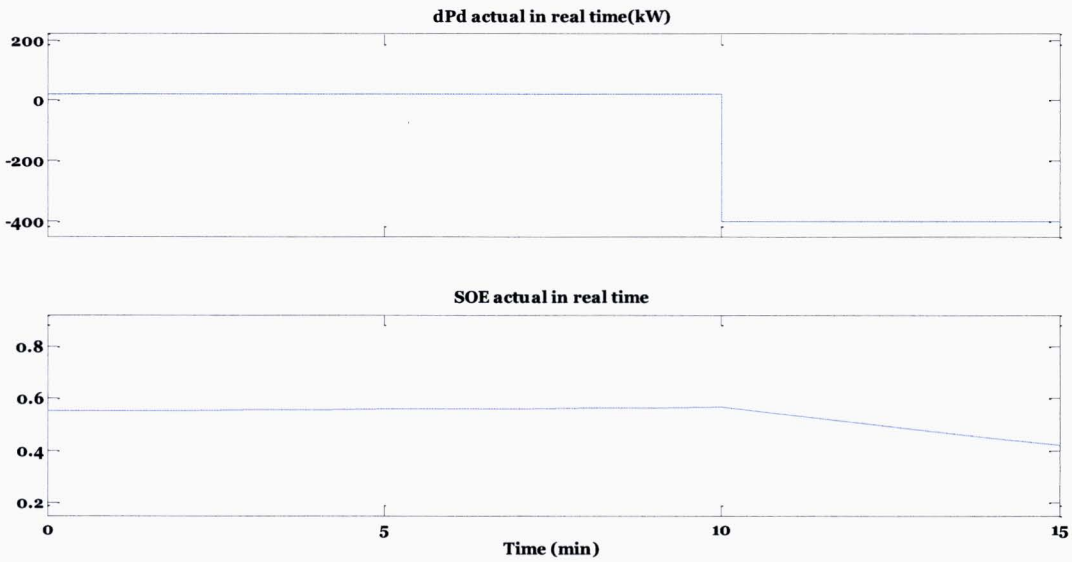

Figure 5.4 Power profile and SoE of the BESS for summer case 3a according to the real time optimisation (30th June, 2012).

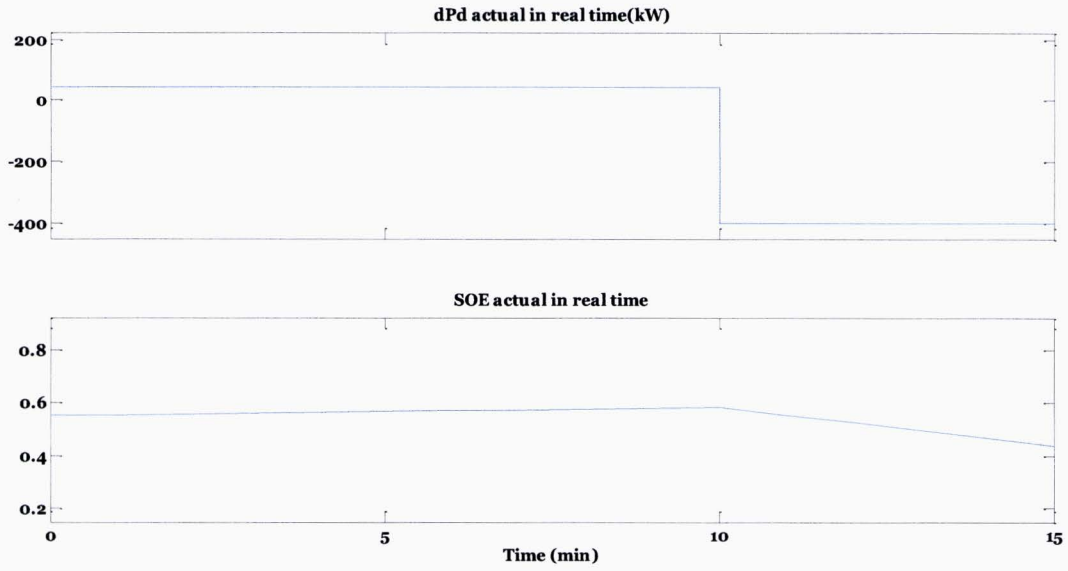

Figure 5.5 Power profile and SoE of the BESS for summer case 3b according to the real time optimisation (30th June, 2012).

5.2.2. Real time case studies for the winter months

The first winter case examines the case of erroneous predictions about the state of the system. The state is forecasted to be 0 instead of 1 and therefore, no energy imbalance is desired. As it is expected, the output of the algorithm, the power devation set-point dP_b is set to 0 to avoid any penalties. Figures 5.6 and 5.7 present the output of the optimisation for this case.

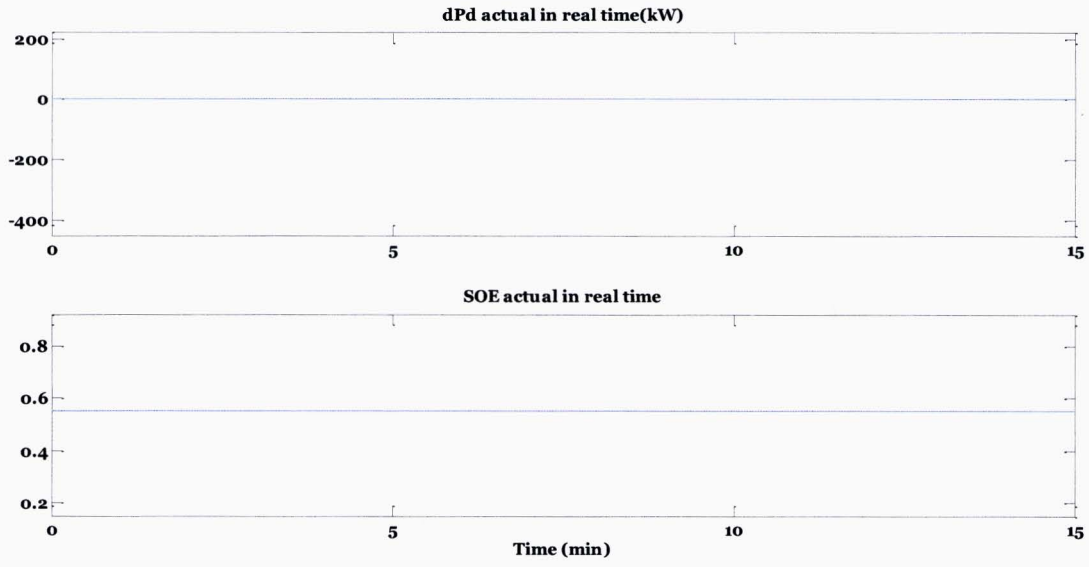

Figure 5.6 Power profile and SoE of the BESS for winter case 1 according to the real time optimisation (12th January, 2012).

At the 2nd case, following an updated prediction, the power profile P_c is larger than expected and as this leads to an undesired imbalance, the dP_b is set to be negative and equal to dP_c to eliminate the overall energy imbalance. Figures 5.7 and 5.8 show the output of the algorithm under these assumptions for both small and large prediction errors (cases 2a and 2b in Table 5.2).

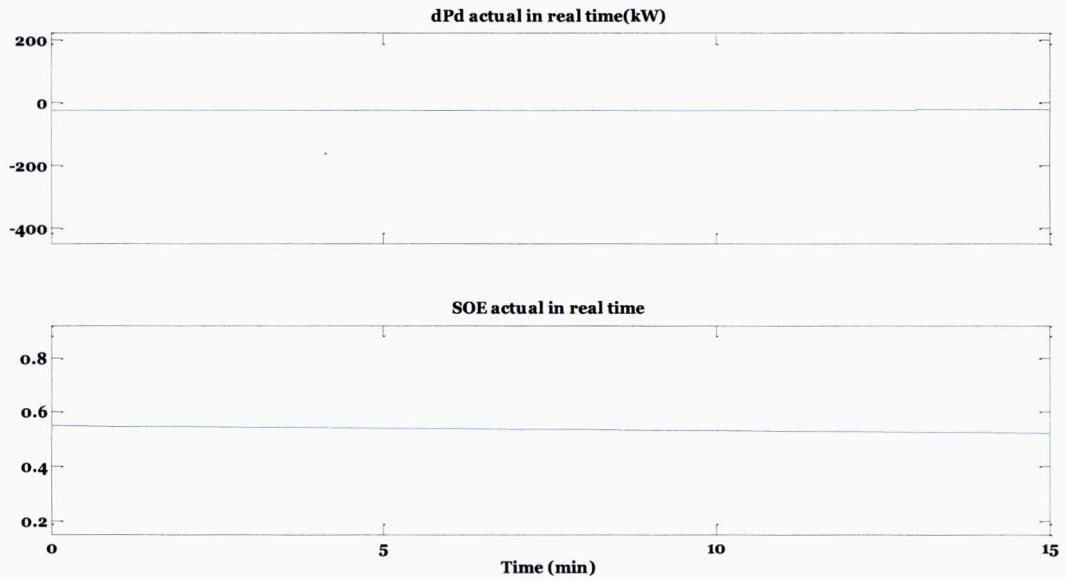

Figure 5.7 Power profile and SoE of the BESS for winter case 2a according to the real time optimisation (12th January, 2012).

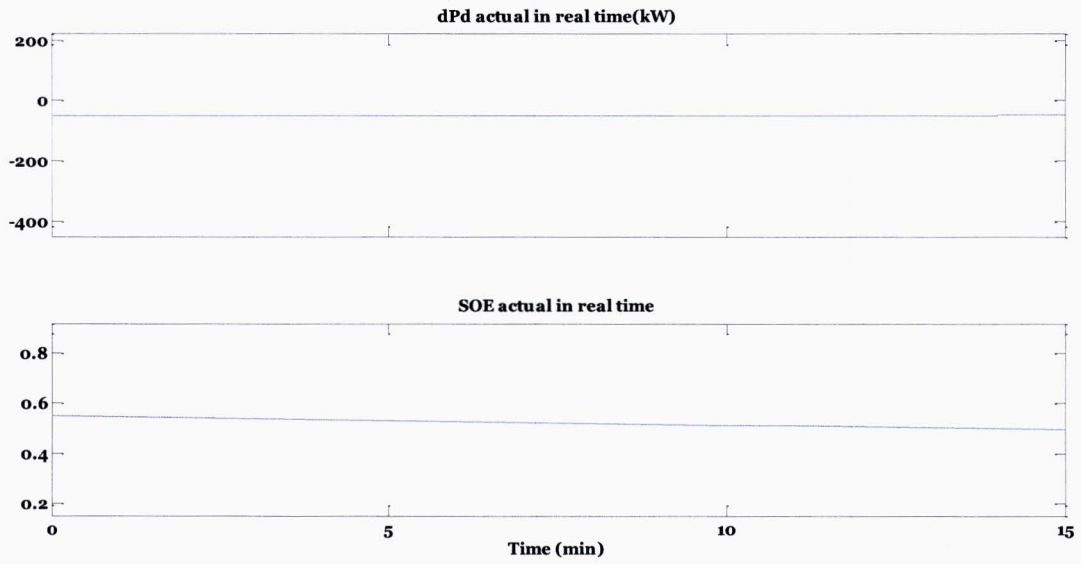

Figure 5.8 Power profile and SoE of the BESS for winter case 2b according to the real time optimisation (12th January, 2012).

Finally, as in section 5.2.1, at the last case the prediction for the state of the system is assumed to be erroneous for the first 10 minutes and at the 11th minute the updated prediction that the aggregator receives is the correct one. Figures 5.9 and 5.10 show how the BESS reacts in that scenario by being discharged with the maximum allowed rate in order to respond to the upwards regulation that is required. The real time algorithm was tested under conditions of updated predictions in real-time and was found to successfully respond in order to increase revenues or to minimise costs.

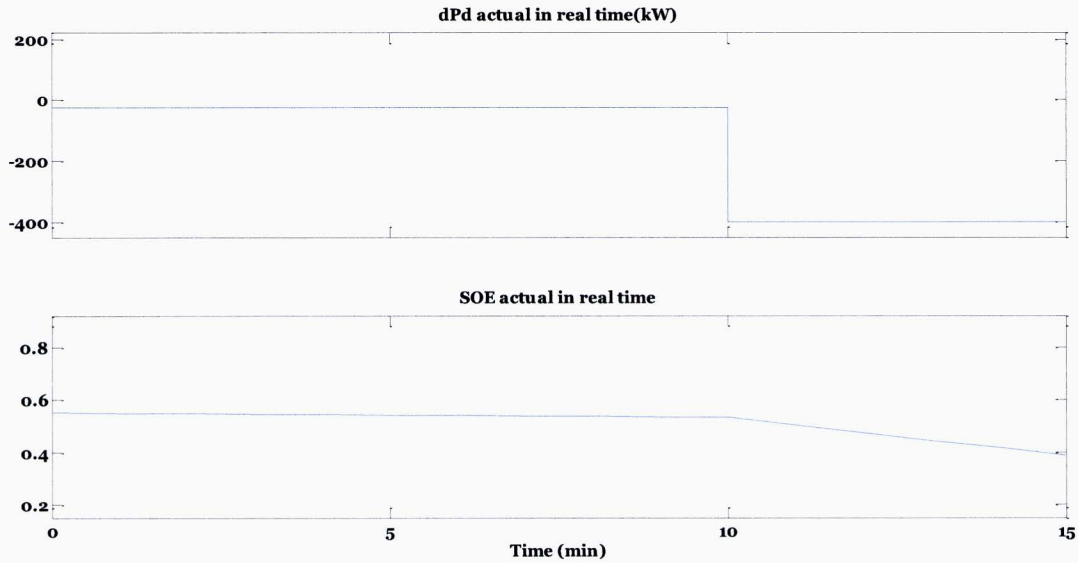

Figure 5.9 Power profile and SoE of the BESS for winter case 3a according to the real time optimisation (12th January, 2012).

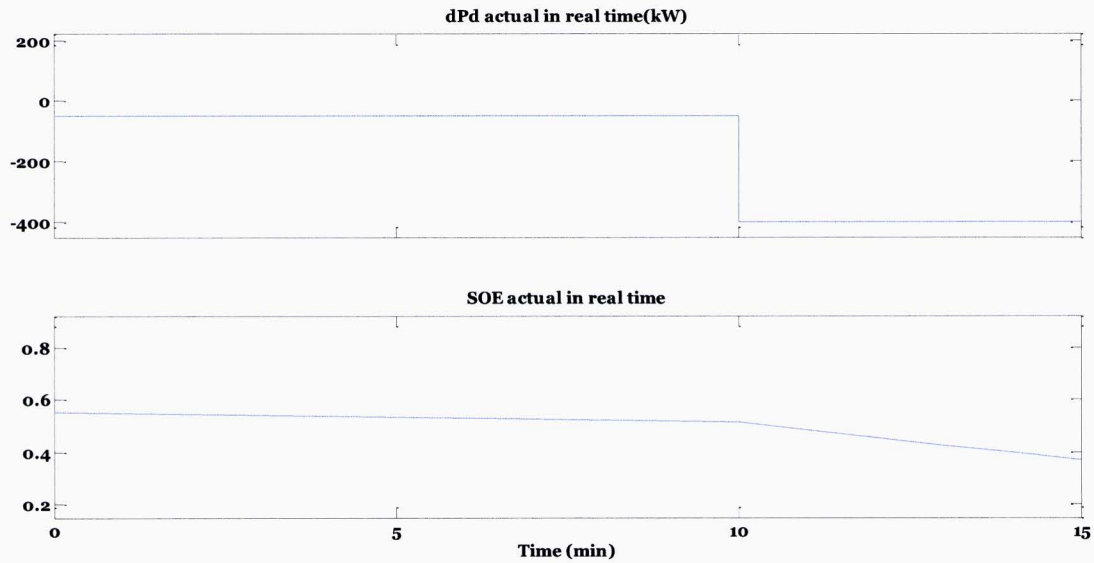

Figure 5.10 Power profile and SoE of the BESS for winter case 3b according to the real time optimisation (12th January, 2012).

Chapter 6 Conclusion

6.1. Discussion and conclusions

In future power systems, characterised by large penetration of renewable energy sources, the use of energy storage technologies can be a significant option to cope with the challenges that the fluctuating nature of wind and solar energy imposes to the system.

Apart from all the services that an energy storage system can provide to the power grid, such as ancillary services, power security or power quality enhancement, many other opportunities arise in the advent of liberalisation of the electricity sector. Different possible markets have appeared in the last years that could provide financial benefits to owners of systems that combines renewable energy sources along with storage devices.

The first market that is examined throughout this work is the APX day-ahead market at which, electricity is traded in the form of day-ahead commitments. The benefits from a storage system at such a market arise purely by following a certain pattern every day, according to which the BESS is being charged at the hours when the electricity prices are low and is being discharged at the hours when the electricity prices are high. In the calculation of the revenues, future prices are assumed to be known beforehand. The potential revenues that the system may have depend greatly on the charging and discharging efficiencies which define the losses of the system. Moreover, another factor that affects the profits from participating in the day-ahead market is the price difference during a day. This price difference varies significantly from year to year, and from day to day, but it can be stated that it is mostly characterised by a decreasing trend in the last decade.

The profit margin that a participant in the day-ahead market may have though, is not as large as the one from participating in the balancing market. The benefits of participating in the imbalance market can be several times larger, and the participant can take advantage of any imbalances that occur from its stochastic procedures (PV generation), the loads of the residential customers or the manipulated output of the BESS and contribute to the system via the passive balancing. The increased revenues occur due to the higher imbalance prices, and the larger number of possible cycles that are performed per day compared with the day-ahead schedule. Despite the fact that such a contribution can be rather profitable, many risks arise considering the accuracy of the predictions. Since the imbalance prices and the state of the system are published later and not in real-time, the aggregator that represents a number of stochastic energy processes has to rely on forecasting algorithms. If the forecasting at the state of the system or the imbalance price at a certain PTU is erroneous, the aggregator may face penalties that are irreversible and this would lead to losses instead of profits.

The risks associated with participation in the balancing market, through passive contribution, are significantly reduced by the adaptable characteristics of the real-time algorithm. The aggregator receives updated predictions on time intervals of one minute and therefore at each minute a new prediction is received for the state of the system, the imbalance prices and the power imbalances from the PV generators and the households' consumption. This leads to a decreased risk as the BESS can react to the updated prediction on real-time and minimise any undesired imbalance or contribute even more to either upwards or downwards regulation. The importance of the real time

algorithm is even bigger when it comes to energy sources that are characterised by variability, intermittency and fluctuation such as solar and wind energy sources. The aggregator receives power measurements and updated predictions for the power profile of all the processes in its portfolio, on a time basis of 1 minute and this can minimise the associated risks.

From a financial point of view, participation in the imbalance market seems to be by far the most interesting market to receive revenues from an energy storage system. The revenues though, are highly affected by the forecasting accuracy of the power generation from the stochastic sources, the electricity prices and the imbalance states of the system. On the other hand, the forecasting is much more accurate for power exchange markets (i.e. the APX day-ahead market) as the prices follow daily regular patterns and therefore are easier to predict.

It is a matter of fact though, that compared with the initial costs of a small-scale battery system, the revenues from participation in the day–ahead auction and the balancing market are still rather small. Until now, distributed battery storage systems are mostly used within pilot programs and research activities and as a result, the capital costs are relatively high. This is also the reason why until now grid-connected electricity storage technologies are seldom economically efficient. This might change over time however, when large scale deployment is applied to battery systems and the costs are likely to be greatly reduced due to economies of scale.

6.2. Recommendations for future research

The current thesis addressed the participation of an aggregator, representing a number of distributed energy resources connected to LV grids, in the day ahead and balancing markets. The work was focused on many specific aspects while other key principles were not examined thoroughly and may need further research and development.

First of all, for the economic assessment, the prediction models throughout the thesis were assumed to be accurate and therefore the predictions were considered perfect both for the APX day-ahead and the imbalance market. In order to optimise the benefits from the participation of the aggregator in the electricity markets, efficient forecasting is required. The development of a forecasting algorithm that could predict the imbalance prices and the state of the system with an efficiency of at least 90% would be the most crucial step in making participation if electricity markets financially viable [34].

Another field that could be further developed is the modelling of the power conversion system. As the contribution of this work does not address thoroughly the modelling of the system, the model that is actually used to describe the losses of the BESS in section 2.2.1.3. is simplified and ignores a whole range of parameters that affect the power losses during charging and discharging modes. A model that takes into account the power rate, the temperature, the SoC and the internal resistance can be formulated for a more exact and accurate representation of the power conversion system and the overall power losses of the BESS.

References

[1] *Moomaw, W., F. Yamba, M. Kamimoto, L. Maurice, J. Nyboer, K. Urama, T. Weir, 2011: Introduction. In IPCC Special Report on Renewable Energy Sources and Climate Change Mitigation [O. Edenhofer, R. Pichs-Madruga, Y. Sokona, K. Seyboth, P. Matschoss, S. Kadner, T. Zwickel, P. Eickemeier, G. Hansen, S. Schlömer, C.von Stechow (eds)], Cambridge University Press, Cambridge, United Kingdom and New York, NY, USA.*

[2] *«Energy in Sweden 2010, Facts and figures» Table 46 Total world energy supply, 1990–2009, Table 48 World power generation by energy resource, 1990–2008 (TWh) nuclear 2,731 TWh in 2008.*

[3] *Nfah, J. M., Ngundam, R., & Tchinda E. M. (2007). Modelling of solar/diesel/battery hybrid power systems for far-north Cameroon. Renewable Energy, 32, 832-844*

[4] *IPCC, 2000b: Climate Change 2007: The Physical Science Basis. Contribution of Working Group I to the Fourth Assessment Report of the Intergovernmental Panel on Climate Change [Solomon, S., D. Qin, M. Manning, Z. Chen, M. Marquis, K.B.M.Tignor and H.L. Miller (eds.)]. Cambridge University Press, Cambridge, United Kingdom and New York, NY, USA, 996 pp.*

[5] *Kankam, Stephen and Boon, Emmanuel K. (2009), 'Energy delivery and utilization for rural development: Lessons from Northern Ghana', Energy for Sustainable Development, 13, 212-18.*

[6] *IPCC, 2011: IPCC Special Report on Renewable Energy Sources and Climate Change Mitigation. Prepared by Working Group III of the Intergovernmental Panel on Climate Change [O. Edenhofer, R. Pichs-Madruga, Y. Sokona, K. Seyboth, P. Matschoss, S. Kadner, T. Zwickel, P. Eickemeier, G. Hansen, S. Schlömer, C. von Stechow (eds)]. Cambridge University Press, Cambridge, United Kingdom and New York, NY, USA, 1075 pp.Available: http://www.ipcc.ch/pdf/special-reports/srren/SRREN_Full_Report.pdf*

[7] *"Electric Energy Storage Systems," Working Group C6.15, Cigre Technical Report, ISBN: 978- 2- 85873- 147-3, April 2011.*

[8] *Z. A. Yamayee, and J. Peschon, "Utility Integration Issues of Residential Photovoltaic Systems," IEEE Trans. Power App. Syst., Vol. PAS-100, No. 5, pp. 2365-2373, May 1981.*

[9] *B. H. Chowdhury, and S. Rahman, "Analysis of interrelationships between photovoltaic power and battery storage for electric utility load management," IEEE Trans Power Syst., Vol. 3, No.3, pp. 900-907, Aug. 1988.*

[10] *M. K. C. Marwali, H. Ma, S. M. Shahidehpour, and K. H. Abdul-Rahman, "Short term generation scheduling in photovoltaic-utility grid with battery storage," IEEE Trans. Power Syst., Vol. 13, No. 3, pp. 1057 – 1062, Aug. 1998.*

[11] *Lampropoulos, W. L. Kling, P. Ribeiro, and J. van den Berg "History of Demand Side Management and Classification of Demand Response Control Schemes," IEEE PES General Meeting, Vancouver, Canada, July 21, 2013.*

[12] *Lampropoulos, W. L. Kling, P. P. J. van den Bosch, P.F.Ribeiro, and J. van den Berg "Criteria for Demand Response Systems," in Proc. of the 9th Conference on the European Energy Market, Florence, Italy, 10-12 May 2012.*

[13] *D. T. Ho, J. F. G. Cobben, S. Bhattacharyya, and W. L. Kling, "Network losses with photovoltaic and storage," in Proc. of the International Conference on Renewable Energies and Power Quality (ICREPQ'10), Granada (Spain), 23rd to 25th March, 2010.*

[14] *R. de Groot, F. van Overbeeke, S. Schouwenaar, and H. Slootweg, "Smart storage in the Enexis LV distribution grid," in Proc. of the 22nd International Conference on Electricity Distribution (C I R E D), Stockholm, 10-13 June 2013.*

[15] *F. van Overbeeke, R. de Groot, J. Bozelie, and H. Slootweg, "Thermal optimization of an integrated LV battery energy storage station," in Proc. of the 22nd International Conference on Electricity Distribution (C I R E D), Stockholm, 10-13 June 2013.*

[16] *User's Manual Lithium-Ion Synerion 24M Module P/N 771187, Doc. No. SDU/EEA/DC/11-0420, 2011 ed., Saft Industrial Battery Group, Bagnolet – France, 2011, pp. 14.*

[17] *Synerion 24M, Medium power lithium-ion module 24V – 2kWh, Doc. No. 21805-2-0412, April 2012 ed., Saft Industrial Battery Group, Bagnolet – France, 2012, pp. 1-2.*

[18] *Internal Market Fact Sheet for the Netherlands, http://ec.europa.eu/energy/energy_policy/doc/factsheets/market/market_nl_en.pdf*

[19] *"Classification of Viable Control Architectures", I.Lampropoulos, E-price Report, Deliverable 1.1., Oct. 2010, Available: http://www.e-price-project.eu/website/files/D1.1.pdf*

[20] *APX Power NL, Day-ahead auction in the Netherlands. [Online]. Available: http://www.apxgroup.com/trading-clearing/day-ahead-auction/*

[21] *Lampropoulos, J. Frunt, A. Virag, F. Nobel, P. P. J. van den Bosch, and W. L. Kling, "Analysis of the market-based service provision for operating reserves in the Netherlands," in Proc. of the 9th Conference on the European Energy Market, Florence, Italy, 10-12 May 2012.*

[22] *J. Frunt, "Analysis of Balancing Requirements in Future Sustainable and Reliable Power Systems", Ph.D. dissertation, Dept. Electrical Eng., Eindhoven University of Technology, 2011.*

[23] *TenneT. (2010, June). The Imbalance Pricing System as at 01-01- 2001, revised per 26-10-2005, TenneT B.V., Version 3.4. [Online]. Available:*
http://www.tennet.org/english/images/imbalanceprice%20incentive%20component%20change_tcm43-11583.pdf

[24] *TenneT 2011, Imbalance Management TenneT, Analysis report, Version 1.0, 28-04-2011, Copyright © 2011 TenneT, E-Bridge & GEN Nederland [Online]. Available:*
http://www.tennettso.de/site/binaries/content/assets/transparency/publications/tender-of-balancing-power/imbalance-management-tennet---analysis-report.pdf

[25] *TenneT web-site, System balance information:*
http://www.tennet.org/english/operational_management/System_data_relating_implementation/system_balance_information/index.aspx

[26] *TenneT Data 2012, Dutch Transmission System Operator, Data export: 'imbalance price' from Jan. 1, 2012 to Dec. 31, 2012, Data accessed May 2013. [Online].Available:*
http://www.tennet.org/english/operational_management/export_data.aspx .

[27] *EM4000. ELEQ b.v., Universal measuring transducer EM4000 product data sheet [Online]. Available: http://www.eleq.com/lmbinaries/ps6eem4000.pdf*

[28] *Rengui Lu, Aochi Yang, Yufeng Xue, Lichao Xu, Chunbo Zhu," Analysis of the key factors affecting the energy efficiency of batteries in electric vehicle", World Electric Vehicle Journal , Vol. 4, pp.9-13,2010.*

[29] *KNMI web-site, KNMI Data Centrum* , https://data.knmi.nl/portal-webapp/KNMI-Datacentrum.html#

[30] *B. M. J. Vonk, P. H. Nguyen, M. O. W. Grond, J. G. Slootweg, and W. L. Kling, "Improving short-term load forecasting for a local energy storage system," in Proc. of the 47th International Universities Power Engineering Conference (UPEC 2012), 4-7 September 2012, London, United Kingdom.*

[31] *J. M. Maciejowski, Predictive Control with Constraints. Prentice Hall, 2002.*

[32] *APX 2013 data* , http://www.apxgroup.com/market-results/apx-power-nl/dashboard/

[33] *Zareipour, H., et al., Electricity market price volatility: The case of Ontario, Energy Policy (2007).*

[34] *Nieuwenhout, F., Hommelberg, M., Schaeffer, G., Kester, J., Visscher, K., "Feasibility of Distributed Electricity Storage". International Journal of Distributed Energy Resources, October-December 2006, ISSI.*

APPENDIX A

DAY-AHEAD PROBLEM - IMPLEMENTATION IN MATLAB

The objective function of the day-ahead problem is given by (3.5)

$$\min_{P_d^{das}(h)} \sum_{h=1}^{24} P_b^{das}(h) \cdot \pi^{prd}(h) = \min_{P_d^{das}(h)} \sum_{h=1}^{24} \left(\frac{1}{\eta_{ch}} \cdot P_{d,ch}^{das}(h) + \eta_{dis} \cdot P_{d,dis}^{das}(h)\right) \cdot \pi^{prd}(h) \quad \text{(A.1)}$$

subject to the following constraints that are given from (3.10)-(3.16):

$$P_{min} \le P_{d,dis}^{das}(h) \le 0, \quad h \in [1,24] \quad \text{(A.2)}$$

$$0 \le P_{d,ch}^{das}(h) \le P_{max}, \quad h \in [1,24] \quad \text{(A.3)}$$

$$P_{d,ch}^{das}(h) \cdot P_{d,dis}^{das}(h) = 0 \quad \text{(A.4)}$$

$$SoE_{min}^{das} \le SoE^{das}(h+1) \le SoE_{max}^{das} \quad \text{(A.5)}$$

$$-400 \text{ kW} - P_c^{prd}(h) \le \eta_{dis} \cdot P_{d,dis}^{das}(h) \quad \text{and} \quad \frac{1}{\eta_{ch}} \cdot P_{d,ch}^{das}(h) \le 400 \text{ kW} - P_c^{prd}(h) \quad \text{(A.6)}$$

In order to solve the day-ahead optimisation problem the **fmincon** command is applied. **Fmincon** is used to find a minimum of constrained nonlinear multivariable functions.

The syntax of **fmincon** is

$$x = fmincon\ (objfun,\ x0,\ A,\ B,\ Aeq,\ Beq,\ lb,\ ub,\ confun)$$

And it finds a constrained minimum of the function **objfun** subject to :

$$A \cdot x \le b,\ A_{eq} \cdot x = b_{eq}$$

$$c(x) \le 0,\ c_{eq}(x) = 0$$

$$ub \le x \le lb$$

The first two equations address the liner constraints, the next two address the nonlinear constraints and the last one sets the bounds of the variable.

In this problem, x vector is the sequence of $P_{d,ch}$, $P_{d,dis}$ .It is a 48X1 vector whose first 24 elements are the $P_{d,ch}$ sequence and the last 24 elements are the $P_{d,dis}$ sequence.

$$x = \begin{pmatrix} P_{d,ch}(1) \\ \vdots \\ P_{d,ch}(24) \\ P_{d,dis}(1) \\ \vdots \\ P_{d,ch}(24) \end{pmatrix}$$

The **objfun** is going to be the objective function described in (A.1) while the only nonlinear constraint (A.4) is going to be defined in the function **confun**.

The other linear constraints are formulated in a compliable form to the **fmincon** structure. The constraint concerning the *SoE* limits (A.5) can be rewritten as $A \cdot x \le b$:

$$\begin{pmatrix} \frac{SoE_{\min} - SoE(0)}{\tau} \cdot E_{nom} \\ \vdots \end{pmatrix} \le \begin{pmatrix} 1 & \cdots & 0 & 1 & \cdots & 0 \\ \vdots & \ddots & \vdots & \vdots & \ddots & \vdots \\ 1 & \cdots & 1 & 1 & \cdots & 1 \end{pmatrix} \cdot \begin{pmatrix} P_{d,ch}(1) \\ \vdots \\ P_{d,ch}(24) \\ P_{d,dis}(1) \\ \vdots \\ P_{d,dis}(1) \end{pmatrix} \le \begin{pmatrix} \frac{SoE_{\max} - SoE(0)}{\tau} \cdot E_{nom} \\ \vdots \end{pmatrix}$$

APPENDIX B

INTRA-HOUR PROBLEM - IMPLEMENTATION IN MATLAB

The objective function of the intra-hour problem can be formulated by (4.2)-(4.5) :

$$\max_{dP_d^{ihs}(q+m|q)} \sum_{m=1}^{48} \Pi(q+m \mid q) \tag{B.1}$$

$$\Pi(q+m \mid q) = \Delta E_{imb}^{prd}(q+m \mid q) \cdot \pi_{imb}^{prd}(q+m \mid q) \tag{B.2}$$

$$\Delta E_{imb}^{prd}(q+m \mid q) = (-dP_b^{ihs}(q+m \mid q) - dP_c^{ihs}(q+m \mid q)) \cdot \tau_s \tag{B.3}$$

Where dP_b^{ihs} can be expressed as:

$$dP_b^{ihs}(l) = \frac{1}{\eta_{ch}} \cdot dP_{d,ch}^{ihs}(l) + \eta_{dis} \cdot dP_{d,dis}^{ihs}(l) \,. \tag{B.4}$$

Subject to the intra-hour constraints

$$P_{min} \le P_{d,dis}^{das}(l) + dP_{d,dis}^{ihs}(l) \le 0 \tag{B.5}$$

$$0 \le P_{d,ch}^{das}(l) + dP_{d,ch}^{ihs}(l) \le P_{max} \tag{B.6}$$

$$P_{d,ch}^{ihs}(l) \cdot P_{d,dis}^{ihs}(l) = 0 \tag{B.7}$$

$$SoE_{min} \le SoE_{mpc}^{ihs}(l+1) \le SoE_{max} \tag{B.8}$$

$$SoE^{ihs}(q+48) = SoE_{ref}^{ihs}(q+48) \tag{B.9}$$

$$\begin{aligned} &-400 \text{ kW} - P_c^{prd}(l) \le \eta_{dis} \cdot P_{d,dis}^{ihs}(l) \\ &\frac{1}{\eta_{ch}} \cdot P_{d,ch}^{ihs}(l) \le 400 \text{ kW} - P_c^{prd}(l) \end{aligned} \tag{B.10}$$

As in the day-ahead schedule, the **fmincon** command is applied in order to solve the intra-hour optimisation problem.

The syntax of **fmincon** is

$$x = fmincon\ (objfun,\ x0,\ A,\ B,\ Aeq,\ Beq,\ lb,\ ub,\ confun)$$

And it finds a constrained minimum of the function **objfun** subject to :

$$A \cdot x \le b,\ A_{eq} \cdot x = b_{eq}$$

$$c(x) \le 0,\ c_{eq}(x) = 0$$

$$ub \le x \le lb$$

In the intra-hour problem, x vector is the sequence of $dP_{d,ch}^{ihs}$, $dP_{d,dis}^{ihs}$. It is a 96X1 vector whose first 48 elements are the $dP_{d,ch}^{ihs}$ sequence and the last 48 elements are the $dP_{d,dis}^{ihs}$ sequence.

$$x = \begin{pmatrix} dP_{d,ch}^{ihs}(1) \\ \vdots \\ dP_{d,ch}^{ihs}(48) \\ dP_{d,dis}^{ihs}(1) \\ \vdots \\ dP_{d,dis}^{ihs}(48) \end{pmatrix}$$

The **objfun** is going to be the objective function described in (B.1)-(B.4). In the function **confun** the nonlinear constraint (B.7) is going to be defined as in the *day-ahead* problem. The other linear constraints are formulated in a compliable form to the **fmincon** structure. The constraint concerning the *SoE* limits (B.8) can be rewritten as $A \cdot x \leq b$

$$\begin{pmatrix} \frac{SoE_{\min} - SoE^{ihs}(0)}{\tau} \cdot E_{nom} + P_d^{das}(1) \\ \vdots \\ \frac{SoE_{\min} - SoE^{ihs}(0)}{\tau} \cdot E_{nom} + P_d^{das}(1) + \ldots + P_d^{das}(48) \end{pmatrix} \leq \begin{pmatrix} 1 & \cdots & 0 & 1 & \cdots & 0 \\ \vdots & \ddots & \vdots & \vdots & \ddots & \vdots \\ 1 & \cdots & 1 & 1 & \cdots & 1 \end{pmatrix} \cdot \begin{pmatrix} dP_{d,ch}^{ihs}(1) \\ \vdots \\ dP_{d,ch}^{ihs}(48) \\ dP_{d,dis}^{ihs}(1) \\ \vdots \\ dP_{d,dis}^{ihs}(48) \end{pmatrix} \leq \begin{pmatrix} \frac{SoE_{\max} - SoE^{ihs}(0)}{\tau} \cdot E_{nom} + P_d^{das}(1) \\ \vdots \\ \frac{SoE_{\max} - SoE^{ihs}(0)}{\tau} \cdot E_{nom} + P_d^{das}(1) + \ldots + P_d^{das}(48) \end{pmatrix}$$

The constraints used to ensure that the constraint (B.9) is not violated can be written as $A_{eq} \cdot x = b_{eq}$

$$(1 \quad \ldots \quad 1) \cdot \begin{pmatrix} dP_{d,ch}^{ihs}(1) \\ \vdots \\ dP_{d,ch}^{ihs}(48) \\ dP_{d,dis}^{ihs}(1) \\ \vdots \\ dP_{d,dis}^{ihs}(48) \end{pmatrix} = \frac{SoE^{das}(48) - SoE^{ihs}(0)}{\tau} \cdot E_{nom} - [P_d^{das}(1) + \ldots + P_d^{das}(48)]$$